

MASS LOSS FROM EVOLVED STARS. III. MASS LOSS RATES FOR FIFTY STARS FROM CO $J = 1-0$ OBSERVATIONS

G. R. KNAPP

Princeton University Observatory and AT & T Bell Laboratories

AND

MARK MORRIS

Astronomy Department, University of California, Los Angeles

Received 1984 June 12; accepted 1984 November 21

ABSTRACT

We present observations at 2.6 mm wavelength of the CO $J = 1-0$ line made with the Bell Laboratories 7 m antenna in the directions of 105 cool, evolved stars having envelopes produced by mass loss. Emission was detected from 50 stars, of which about half are M-type Mira variables, half are carbon or S stars, and two are supergiants. Twenty of these envelopes are detected for the first time in the CO(1-0) line, including the OH/IR supergiant IRC + 10420 and the OH maser-bipolar nebula OH 231.8+4.2. The data are used to derive values for the stellar systemic velocity, the terminal outflow velocity of the wind, and the mass loss rate \dot{M} for the envelopes.

The values of \dot{M} were found by matching the observed line profiles to those calculated from detailed models of the circumstellar envelopes. The data suggest that $[\text{CO}]/[\text{H}_2]$ is about 3 times higher in the carbon stars than in the M-type Mira variables, whose relative C and O abundances are similar to the solar values. For OH/IR stars, the values of \dot{M} determined from CO observations agree very well in almost all cases with those found from observations of the maser shell size. The values of \dot{M} derived from CO observations cover a range of $\sim 10^{-7}$ to a few $\times 10^{-4} M_{\odot} \text{ yr}^{-1}$. A preliminary estimate of the total galactic rate of mass return to the interstellar medium by such stars gives $\dot{M}_T \sim 0.3 M_{\odot} \text{ yr}^{-1}$.

Subject headings: stars: abundances — stars: carbon — stars: circumstellar shells — stars: long-period variables — stars: mass loss

I. INTRODUCTION

This is Paper III in a series investigating the properties of the circumstellar envelopes produced by mass loss from evolved stars. These envelopes are of importance both because of their role in the cycling and processing of the interstellar gas and because of what they can tell us about the influence of copious mass loss on the evolution of the star. Further, it is becoming increasingly evident that, at least for stars with $M \lesssim 5-6 M_{\odot}$, the copious mass loss immediately precedes the production of a planetary nebula (e.g., Zuckerman 1978).

In Paper I of this series (Knapp *et al.* 1982) observations were given of the CO $J = 2-1$ line of a sample of circumstellar envelopes. From these observations, approximate mass loss rates were derived using simple models. The high spatial resolution available with the CO $J = 2-1$ line allowed an estimate of the radii of some envelopes to be made, thus providing a minimum estimate of the total envelope mass. The implications of the large values of the mass loss rate for planetary nebula evolution and the results of a radio continuum survey of pre-planetary nebula envelopes were discussed in Paper II (Spergel, Giuliani, and Knapp 1983). In the present paper, we describe observations of 105 evolved stars in the $J = 1-0$ line of $^{12}\text{C}^{16}\text{O}$ (hereafter CO); emission was detected from 50 of them. From these data we calculate the physical parameters of the envelopes: the systemic stellar velocity, the terminal outflow velocity of the wind, and the loss rate of CO molecules. The first two quantities may be found directly from the data by the fitting of a simple line-shape function. Finding the last quantity requires knowledge of the distance to the star as well as the use of a model of line formation in the envelope to fit the

observed emission profile. If the model is sufficiently detailed or if independent data exist on the relative CO abundance, the total mass loss rate can be determined. The goal of the present paper is to derive physical parameters as accurately and uniformly as possible for a large sample of objects. Analysis of these results will be described in future work.

In the next section, the observations are described, and values for the peak line temperature, stellar velocity, and wind outflow velocity are given for the detected envelopes, whose line profiles are presented in Figure 24, which appears at the end of this paper. In § II, we also describe monitoring observations of the CO emission from CIT 6 and the observation of the 115.4 GHz line of SiC₂ in IRC + 10216 and CIT 6. In § III, we describe calculations of CO emission from model circumstellar envelopes, which are used to derive values of the mean mass loss rates. The results and their reliability are critically discussed in § IV. In § IV we also discuss the rate of return of gas to the interstellar medium from evolved stars, and in § V we give the conclusions of this work.

II. OBSERVATIONS

a) Equipment and Observations

The observations were made in the winters of 1980/1981 and 1982/1983 using the 7 m antenna of Bell Laboratories at Holmdel, New Jersey. The telescope half-power beamwidth is measured to be 100" at 115 GHz. The pointing and tracking were found to be accurate to about 20". The spectral line receiver used for these observations was a filter bank consisting of 256 0.25 MHz and 512 1 MHz channels. Half of the 0.25 MHz filter bank can be processed by a spectrum expander to give

higher frequency resolution. For a few of the observations described herein, a resolution of 100 kHz was used, but for the great majority of the observations, the observed parameters were taken from the 256×0.25 MHz filters.

The receiver response (antenna temperature scale) was calibrated every hour or so during the observations by terminating the optical path at the receiver using hot (room temperature) and cold (liquid nitrogen) loads. The temperature of the atmospheric emission was measured at the same time, and the attenuation found by fitting to an atmospheric model. Almost all of the observations described herein were made during cold, clear weather, with the attenuation typically 0.4–0.7 at the zenith.

The observed antenna temperatures were corrected for atmospheric attenuation and spillover and finally corrected for the beam efficiency of 85% (which was measured using observations of Jupiter, whose uniform-disk brightness temperature was taken to be 170 K). This calibration involves the assumption that the source size is of the same order as that of Jupiter and of the telescope half-power beamwidth, i.e., in the range of $1'–2'$ or less (cf. the discussion in Paper I). The resulting temperatures are thus expressed in units of T_A^* , the Rayleigh-Jeans equivalent brightness temperature seen by a perfect antenna above the atmosphere (Phillips, Jefferts, and Wannier 1974).

In 1980–1981, a cooled Schottky-barrier diode receiver at the Cassegrain focus of the telescope was used for the observations. This is a WR-8 version of the WR-12 receiver described by Linke, Schneider, and Cho (1978). For the 1982/1983 observations, a liquid helium-cooled SIS receiver (Phillips *et al.* 1981) mounted at the Nasmyth focus was used. The efficiency of the telescope/receiver combination was the same to 2% in both cases. The single-sideband receiver temperatures were typically 340 K for the diode receiver and 280 K for the SIS receiver. The effective value of the system temperature (the equivalent single-sideband system temperature for a perfect telescope above the atmosphere) was $\sim 700–1200$ K for these observations, depending on the zenith angle at which the source was observed.

The observations were made in a position-switched mode, with individual observations lasting about 10 minutes. Each observation was examined, and those few with nonlinear baselines were rejected. The satisfactory observations were averaged and linear baselines removed, using the velocity range(s) determined to be free of CO emission. The reference points for position switching were generally chosen to be offset by $\pm 10'$ in right ascension from the stellar position. For some of the sources which are close to the galactic plane and/or have velocities close to 0 km s^{-1} , the source and reference positions sometimes contained emission from galactic molecular clouds, resulting in confusion with the observed or expected circumstellar envelope emission.

b) Sample of Stars

A sample of 105 stars was observed, with typical total integration times of 5 hours for each object. The stars were selected according to several criteria. The most important list was that of stars known to be CO sources. These previously detected stars were included because, as will be discussed in § IV, the published data provide insufficient information for the calculation of mass loss rates in most cases. IRC +10216 was first detected by Solomon *et al.* (1971) and observed with greater sensitivity by Kuiper *et al.* (1976). CIT 6 was detected by Wilson, Schwartz, and Epstein (1973), and more sensitive

observations are given by Mufson and Liszt (1975), Knapp, Kuiper, and Zuckerman (1979), and Zuckerman (1981). Frogel, Dickinson, and Hyland (1975) detected IRC +10450, as did Zuckerman *et al.* (1977), who also report detections of IRC +10011, R Scl, IRC +50096, NML Tau, CRL 865, V Hya, IRC +20370, V Cyg, IRC +40485, and CRL 3068. Emission from IRC +60150, IRC –10236, CRL 2135, CRL 2155, CRL 2199, and W Aql was found by Zuckerman *et al.* (1978). NGC 7027 was first detected by Mufson, Lyon, and Marioni (1975), and more recent observations were reported by Thronson (1983). R Cas was detected by Lambert and Vanden Bout (1978). Lo and Bechis (1976) detected CRL 2688 and CRL 618, and Lo and Bechis (1977) reported detections of ρ Cet, VY CMA, S CMi, RS Cnc, IRC +20326, and χ Cyg. IRC +40004, IRC +10365, IRC –10529, and IRC +70066 were detected by Zuckerman (1981). In addition, four stars have been detected only in the CO(2–1) line: α Ori (Knapp, Phillips, and Huggins 1980) and R Leo, R LMi, and RX Boo (Paper I). In the above list of objects, the detections of IRC +40485, S CMi, R LMi, and IRC +70066 are considered tentative. Upper limits for the CO(1–0) emission from many other stars are given by these authors.

In the present paper, we report observations of all of these stars except CRL 2135, and confirm all of the detections except those of α Ori, VY CMA, S CMi, and R LMi. For α Ori, we have only a very tentative detection of the CO(1–0) line. For VY CMA, the narrow line reported by Lo and Bechis (1977) is present and likely arises from the large molecular cloud with which the star is associated (Lada and Reid 1978); we find no emission as broad as the thermal SiO emission line from the star (Buhl *et al.* 1975; Morris *et al.* 1979). For S CMi, our observations are sensitive enough to be in disagreement with the tentative detection by Lo and Bechis (1977). Our observation of R LMi is not sensitive enough to conflict with the results in Paper I. For the remaining stars, the present observations are in substantial agreement with previous work; the comparison of the data will be further discussed in § IV of this paper.

Other candidates for observation were selected from lists of (1) nearby 1612 MHz OH masers; (2) objects in the AFGL catalog (Price and Walker 1976) identified with carbon stars (Altamore *et al.* 1980); (3) the “reddest stars in the 2μ sky survey” (Kleinmann and Payne-Gaposchkin 1979); (4) nearby Mira variables (Bowers and Hagen 1984); and (5) thermal SiO emitters (Morris *et al.* 1979). In all cases, nearby objects with accurately known positions were chosen. In all, 71 additional stars were observed, and 19 of them were detected.

If the velocity of the star was known, the frequency of observation was set at this velocity, and was otherwise centered at 0 km s^{-1} (LSR). The coverage of the 250 kHz filter banks is $\sim \pm 80 \text{ km s}^{-1}$. However, the chance of missing a star with a high velocity is negligible, since observations were simultaneously made with the 1 MHz filter bank, which covers a velocity range of $\sim 1300 \text{ km s}^{-1}$.

In all, CO(1–0) emission was detected from 50 stars. The line profiles are given in Figure 24. The emission from α Ori is very weak, and only an estimate of the CO flux (or its upper limit) can be made. The detections of α Ori, VY 2–2, R Lep, RT Vir, IRC +10420, Y CVn, and IRC +40483 are tentative.

c) Results

The results are summarized in Figure 24 and in Table 1. The first three columns of Table 1 list the standard name of the star

TABLE 1
CO(1-0) OBSERVATIONS OF EVOLVED STARS

Star	R.A. (1950)	Decl. (1950)	rms (K)	Line Flux (K km s ⁻¹)	T _∗ (K)	V _c (LSR) (km s ⁻¹)	V _o (km s ⁻¹)	Notes
IRC +40004	00 ^h 04 ^m 18 ^s	+42°48'21"	0.04	2.9 ± 0.3	0.09 ± 0.01	-19.7 ± 1.2	24.2 ± 1.5	
VX And	00 17 15	+44 25 54	0.08	
R And	00 21 23	+38 18 02	0.05	1.4 ± 0.2	0.13 ± 0.01	-16.0 ± 0.4	8.7 ± 0.4	
IRC +10011	01 03 48	+12 19 45	0.09	5.6 ± 0.6	0.18 ± 0.01	+9.5 ± 0.8	23.0 ± 0.9	
IRC +50030	01 08 03	+53 27 53	0.04	
Z Psc	01 13 18	+25 30 41	0.05	
R Scl	01 24 40	-32 48 07	0.13	10.8 ± 0.8	0.32 ± 0.02	-17.7 ± 1.2	24.7 ± 1.7	
OH 127.8+0.0	01 30 28	+62 11 31	0.05	
NGC 650	01 39 10	+51 19 22	0.05	
W And	02 14 23	+44 04 29	0.03	
o Cet	02 16 49	-03 12 12	0.04	2.6 ± 0.1	0.38 ± 0.01	+46.8 ± 0.1	6.0 ± 0.2	1, 2
S Per	02 19 15	+58 21 33	0.03	
CRL 341	02 29 21	+57 48 53	0.03	3
U Ari	03 08 15	+14 36 48	0.07	
CRL 482	03 18 39	+70 16 47	0.04	2.4 ± 0.2	0.11 ± 0.01	-12.2 ± 1.3	16.0 ± 2.1	4, 5
IRC +50096	03 22 59	+47 21 19	0.07	4.7 ± 0.3	0.21 ± 0.01	-17.2 ± 0.7	16.8 ± 0.9	
IRC +40070	03 48 55	+39 43 48	0.05	3
NML Tau	03 50 44	+11 15 31	0.04	6.0 ± 0.2	0.20 ± 0.01	+34.6 ± 0.4	22.0 ± 0.6	
IRC +60144	04 30 49	+62 10 11	0.05	3.2 ± 0.2	0.12 ± 0.01	-44.5 ± 0.9	20.4 ± 1.5	
CRL 618	04 39 34	+36 01 15	0.12	12.3 ± 0.7	0.43 ± 0.02	-21.3 ± 0.6	21.5 ± 0.9	
IRC +50130	04 50 25	+49 49 05	0.10	
IRC +60150	04 56 43	+56 06 48	0.04	2.0 ± 0.2	0.12 ± 0.01	+13.4 ± 0.3	12.5 ± 0.1	4, 5
R Lep	04 57 20	-14 52 47	0.05	(2.5 ± 0.3)	(0.09 ± 0.01)	(+15.6 ± 1.4)	(20.5 ± 1.6)	
IRC +50137	05 07 20	+52 48 53	0.05	1.6 ± 0.3	0.08 ± 0.01	+6.8 ± 1.3	14.7 ± 1.9	4, 5
R Aur	05 13 15	+53 31 57	0.03	0.9 ± 0.1	0.06 ± 0.01	-0.4 ± 0.6	10.9 ± 0.6	
IRC +30114	05 23 47	+34 06 53	0.06	
IC 418	05 25 10	-12 44 15	0.06	
CRL 799	05 37 56	+13 45 48	0.03	
U Aur	05 38 52	+32 01 06	0.05	
CRL 809	05 40 33	+32 40 48	0.05	3
IRC +70066	05 41 08	+69 57 15	0.04	2.2 ± 0.2	0.08 ± 0.01	+0.9 ± 1.2	21.1 ± 1.2	
α Ori	05 52 28	+07 23 58	0.02	(0.3 ± 0.1)	
U Ori	05 52 51	+20 10 06	0.03	
V Cam	05 55 58	+74 30 23	0.05	
CRL 865	06 01 18	+07 26 03	0.04	3.3 ± 0.2	0.16 ± 0.01	+42.3 ± 0.4	15.3 ± 0.4	
IRC +60169	06 30 01	+60 58 49	0.03	1.9 ± 0.1	0.08 ± 0.01	-22.3 ± 0.7	16.9 ± 0.5	
R Gem	07 04 21	+22 46 57	0.04	
W CMa	07 05 43	-11 50 38	0.13	
VY CMa	07 20 55	-25 40 11	0.05	3, 6
S CMi	07 30 00	+08 25 35	0.03	
OH 231.8+4.2	07 39 59	-14 36 11	0.02	3.5 ± 0.4	0.04 ± 0.004	+25.0 ± 4.4	68.5 ± 3.5	6
R Cnc	08 13 49	+11 52 53	0.03	
RY Hya	08 17 31	+02 55 42	0.04	
X Cnc	08 52 34	+17 25 22	0.05	
RS Cnc	09 07 38	+31 10 06	0.03	1.0 ± 0.1	0.12 ± 0.01	+6.8 ± 0.3	5.3 ± 0.4	
R LMi	09 42 35	+34 44 33	0.03	
IRC -20197	09 42 56	-21 48 05	0.12	
R Leo	09 45 15	+13 30 45	0.03	0.3 ± 0.1	0.05 ± 0.01	-2.5 ± 0.5	4.0 ± 0.6	
IRC +10216	09 45 15	+13 30 45	0.05	123.1 ± 0.2	5.10 ± 0.02	-26.2 ± 0.0	15.2 ± 0.0	7
CIT 6	10 13 12	+30 49 24	0.02	19.9 ± 0.1	0.74 ± 0.01	-1.8 ± 0.2	16.9 ± 0.1	7
IRC -10236	10 14 35	-14 24 31	0.04	3.0 ± 0.2	0.21 ± 0.01	+3.3 ± 0.3	10.9 ± 0.4	
R UMa	10 41 08	+69 02 19	0.04	
VY UMa	10 41 37	+67 40 26	0.04	
V Hya	10 49 11	-20 59 04	0.12	5.4 ± 0.5	0.22 ± 0.02	-13.8 ± 1.2	20.9 ± 1.1	
R Com	12 01 42	+19 03 38	0.04	
SS Vir	12 22 41	+01 02 50	0.04	
R Vir	12 35 58	+07 15 47	0.03	
Y CVn	12 42 47	+45 42 47	0.03	(0.7 ± 0.1)	(0.06 ± 0.01)	(+21.7 ± 0.3)	(7.9 ± 0.3)	
RU Vir	12 44 46	+04 25 02	0.04	1.4 ± 0.2	0.07 ± 0.01	+0.5 ± 1.0	16.9 ± 1.3	
U CVn	12 44 57	+38 38 23	0.07	
RT Vir	13 00 06	+05 27 14	0.06	(1.3 ± 0.2)	(0.08 ± 0.01)	(+15.4 ± 0.4)	(11.3 ± 0.5)	
R Hya	13 26 58	-23 01 24	0.08	
W Hya	13 46 12	-28 07 05	0.13	
RX Boo	14 21 57	+25 55 49	0.02	1.4 ± 0.1	0.09 ± 0.01	+1.6 ± 0.4	11.5 ± 0.6	
RS Vir	14 24 45	+04 53 54	0.05	
S CrB	15 19 22	+31 32 46	0.03	
WX Ser	15 25 32	+19 44 13	0.03	
S UMi	15 31 27	+78 48 10	0.08	
R Ser	15 48 23	+15 17 01	0.07	
U Her	16 23 35	+19 00 18	0.04	
IRC +30292	16 25 59	+34 54 36	0.06	

TABLE 1.—Continued

Star	R.A. (1950)	Decl. (1950)	rms (K)	Line Flux (K km s ⁻¹)	T _A [*] (K)	V _c (LSR) (km s ⁻¹)	V _o (km s ⁻¹)	Notes
IRC + 10322	17 ^h 11 ^m 56 ^s	+08°59'22"	0.05	
IRC + 20326	17 29 42	+17 47 35	0.11	5.4 ± 0.5	0.23 ± 0.02	-5.0 ± 0.8	17.5 ± 0.7	
T Dra	17 55 37	+58 13 24	0.04	1.3 ± 0.1	0.07 ± 0.01	-12.3 ± 0.7	14.0 ± 0.9	
IRC - 10396	18 04 05	-09 41 37	0.05	3
CRL 2154	18 23 57	-06 55 34	0.10	3
CRL 2155	18 24 01	+23 27 01	0.06	3.6 ± 0.3	0.18 ± 0.01	+60.4 ± 0.6	15.1 ± 0.8	
IRC + 00351	18 24 25	+01 07 14	0.04	
CRL 2199	18 33 20	+05 33 17	0.06	1.9 ± 0.2	0.16 ± 0.02	+36.0 ± 0.6	8.0 ± 0.4	
IRC + 10365	18 34 58	+10 23 04	0.05	3.0 ± 0.2	0.13 ± 0.01	-31.4 ± 0.5	16.7 ± 0.4	
IRC + 20370	18 39 42	+17 38 16	0.07	6.9 ± 0.4	0.32 ± 0.01	-0.7 ± 0.4	15.6 ± 0.6	
W Aql	19 12 42	-07 08 07	0.06	9.6 ± 0.3	0.36 ± 0.01	-25.0 ± 0.4	19.9 ± 0.5	
Vy 2-2	19 21 59	+09 47 59	0.02	(0.3 ± 0.1)	(0.02 ± 0.004)	(-44.3 ± 1.0)	(12.1 ± 1.0)	
IRC + 10420	19 24 27	+11 15 11	0.03	(2.4 ± 0.3)	(0.03 ± 0.005)	(+80.9 ± 5.4)	(51.7 ± 7.3)	4
χ Cyg	19 48 39	+32 47 12	0.06	4.0 ± 0.2	0.29 ± 0.01	+9.7 ± 0.3	10.2 ± 0.4	
IRC - 10529	20 07 48	-06 25 02	0.10	6.7 ± 0.6	0.30 ± 0.02	-15.1 ± 0.7	15.8 ± 0.9	
V Cyg	20 39 41	+47 57 44	0.06	6.5 ± 0.3	0.37 ± 0.01	+13.3 ± 0.4	13.1 ± 0.5	4, 5
NML Cyg	20 44 34	+39 55 56	0.08	3
CRL 2688	21 00 20	+36 29 43	0.13	33.7 ± 0.7	1.27 ± 0.02	-36.0 ± 0.2	19.7 ± 0.3	
IRC + 00499	21 03 18	-00 24 48	0.06	2.0 ± 0.3	0.09 ± 0.01	+1.5 ± 0.5	16.4 ± 0.6	
NGC 7027	21 05 09	+42 02 02	0.13	23.1 ± 0.6	0.98 ± 0.03	+24.8 ± 0.3	17.9 ± 0.2	
T Cep	21 08 53	+68 17 13	0.05	
IRC + 40483	21 25 25	+36 28 53	0.03	(0.9 ± 0.1)	(0.04 ± 0.004)	(+42.4 ± 1.5)	(18.0 ± 1.1)	
IRC + 40485	21 32 06	+38 51 00	0.05	2.6 ± 0.2	0.11 ± 0.01	-4.5 ± 1.1	14.9 ± 1.4	
μ Cep	21 41 59	+58 33 00	0.04	
CRL 2901	22 24 04	+60 04 29	0.03	3
MY Cep	22 52 32	+60 33 36	0.04	3
R Peg	23 04 08	+10 16 21	0.06	
CRL 3068	23 16 43	+16 55 07	0.06	6.9 ± 0.3	0.36 ± 0.01	-31.1 ± 0.2	14.5 ± 0.2	
NGC 7662	23 23 29	+42 15 36	0.11	
CRL 3099	23 25 45	+10 38 07	0.04	2.1 ± 0.1	0.16 ± 0.01	+46.6 ± 0.4	10.1 ± 0.5	
IRC + 40540	23 32 00	+43 16 17	0.05	9.2 ± 0.2	0.47 ± 0.01	-14.7 ± 0.3	14.7 ± 0.3	
R Aqr	23 41 14	-15 33 41	0.08	
R Cas	23 55 52	+51 06 36	0.04	1.9 ± 0.2	0.12 ± 0.01	+25.7 ± 0.5	12.3 ± 0.6	
WZ Cas	23 58 42	+60 04 36	0.03	

NOTES.—(1) Parameters from Gaussian fit. (2) Observed with 100 kHz filters. (3) Galactic emission either at expected velocity of star or near 0 km s⁻¹. (4) Confusion by galactic CO emission. (5) Line flux calculated from parameters of parabolic fit. (6) Parameters from 1 MHz filter bank. (7) Flattened parabola fitted to data. See text, § IIc. (8) The quoted errors are internal errors only. The systematic errors in the line flux and T_A^{*} are ~20%. The errors in V_c and V_o are increased by at least a factor of 2 for weak detections by baseline ripple.

and the 1950 position used in the observations. Column (4) gives the rms noise in the 250 kHz filter banks. Since the 1 MHz filter bank observations were examined also, upper limits may be calculated assuming half of the value of the rms noise given in Table 1. Next, in column (5), is the integrated flux in the CO line found by summing over the velocity range of the observed emission, in units of K km s⁻¹. Finally, in columns (6), (7), and (8) we list the peak emission temperature T_A^{*}(peak), the central velocity V_c of the line, and the terminal outflow velocity of the envelope, V_o.

The last three quantities were found as follows. If the envelope is spherically symmetric with constant outflow velocity, unresolved by the instrumental beam, and optically thick everywhere in the CO(1-0) line, the resulting emission line is parabolic in shape (Morris 1975, 1980). The observed line shape allows strong constraints on the parameters of the circumstellar envelope to be set (Morris 1980); for the present observations, this is further discussed in the next section. The line profiles, which are presented in Figure 24, were examined and their line shapes indeed found to be consistent with being parabolic, within the noise, in most cases. The line shape may then be described by

$$T_A^*(V) = T_A^*(\text{peak}) \left[1 - \left(\frac{V - V_c}{V_o} \right)^2 \right], \quad |V - V_c| < V_o$$

$$= 0, \quad |V - V_c| \geq V_o. \quad (1)$$

A function of this form was fitted to the observed data to give the results in Table 1. [The quantity T_A^{*}(peak) is referred to as T_A^{*} for brevity.] The fitting was done using a grid-search least squares technique (Bevington 1969, p. 220). In each case, the fitted line was plotted on top of the data for visual examination of the goodness of fit. The residuals of the fit were also examined. An example of the calculated fit for the observation of CRL 3099 is shown in Figure 1. The exception to the above is Mira, whose profile (see Fig. 24) was Gaussian in appearance. The parameters in Table 1 are those of a Gaussian fitted to the data for Mira.

The flux in a parabolic emission line is given by 4T_A^{*}V_o/3. For a few of the observations, galactic emission, either at the position of the star or in the reference positions, contaminates the observed line profile. In these cases (indicated in the notes to Table 1), the line area listed is calculated from the parameters of the parabola fitted to the uncontaminated portion of the profile.

The parabolic line shape can become flatter on top either as a result of resolution by the telescope or because the emission is optically thin (Morris 1975, 1980). The former is known to occur for IRC +10216 (Kuiper *et al.* 1976) and the latter for CIT 6 (Knapp, Kuiper, and Zuckerman 1979). For both of these objects, we have acquired profiles with a high signal-to-noise ratio (see § II d) which are observed to be flat-topped, and equation (1) does not provide a good fit to the observations. A

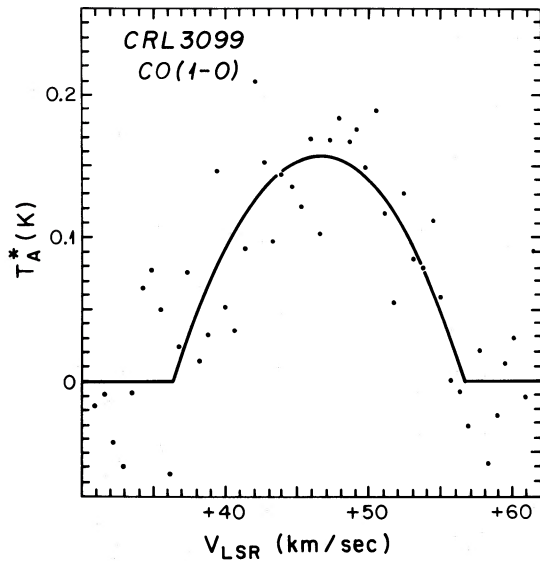


FIG. 1.—The CO(1-0) line profile of CRL 3099 observed with the Bell Laboratories 7 m antenna. The ordinate is Rayleigh-Jeans equivalent brightness temperature T_A^* in K, and the abscissa is velocity with respect to the LSR in km s^{-1} . The observed points are shown by dots, and a parabolic profile fitted by least squares by the solid line.

flat-topped parabola may be approximately parameterized by replacing the first part of equation (1) by

$$T_A^*(V) = T_0 \left[1 - \exp \left\{ -\alpha \left[1 - \left(\frac{V - V_c}{V_o} \right)^2 \right] \right\} \right] (1 - e^{-\alpha})^{-1}, \quad (2)$$

where $T_0 = T_A^*(\text{peak})$ (e.g., Kuiper *et al.* 1976; Knapp, Kuiper, and Zuckerman 1979). A function of this form was fitted to the profiles for IRC + 10216 and CIT 6 using a similar grid-search method, and provides excellent fits to the data (see Figs. 2 and 3). The calculated values are listed in Table 2, and the resulting

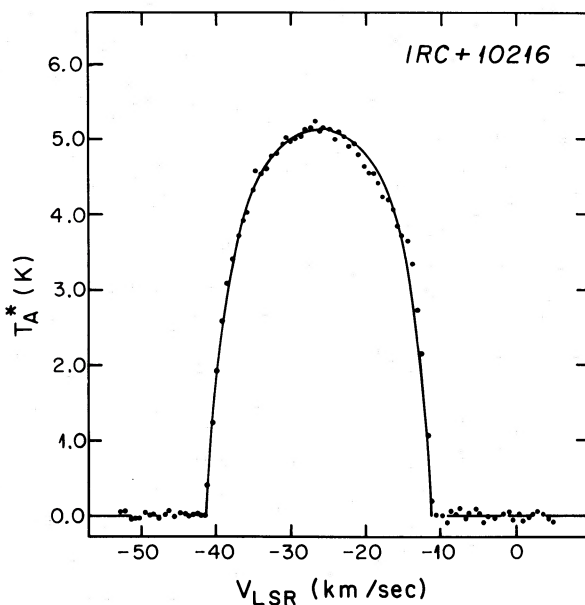


FIG. 2.—The CO(1-0) line profile of IRC + 10216. The fitted curve is a flattened parabola (see text).

TABLE 2
FOUR-PARAMETER FITS TO THE CO(1-0) LINE PROFILES OF
IRC + 10216 AND CIT 6

Parameter	IRC + 10216	CIT 6
T_{peak} (K)	5.76 ± 0.01	0.86 ± 0.005
α	2.2 ± 1.0	2.0 ± 1.0
T_0 (K)	5.10 ± 0.02	0.74 ± 0.01
V_o (km s^{-1})	15.20 ± 0.02	16.91 ± 0.06
V_c (km s^{-1})	-26.23 ± 0.02	-1.78 ± 0.06

NOTE.—Quoted errors are internal statistical errors only. The systematic errors in the temperature scale are $\sim 20\%$.

values of V_c , V_o , and $T_A^*(\text{peak})$ in the appropriate columns in Table 1. As can be seen, the fitting of equation (2) optimizes, to first order, the product αT_0 , and observations with a very high signal-to-noise ratio are needed if equation (2) is to be more useful than equation (1). In the present set of data, only the profiles of IRC + 10216 and CIT 6 fulfill this criterion. Note, however, that if a profile is not parabolic but is flat-topped, the use of equation (1) rather than equation (2) can result in V_o being overestimated.

The errors quoted in Tables 1 and 2 are internal errors found from the fitting procedure. Systematic errors due, for example, to calibration uncertainties and baseline ripple are likely to be much larger, of order 20% in the peak temperatures and line fluxes, and up to twice the quoted values for the errors in V_o and V_c for weak lines.

For IRC + 10216, the value of V_c in Table 2 agrees very well with values for several molecules given by Olofsson *et al.*

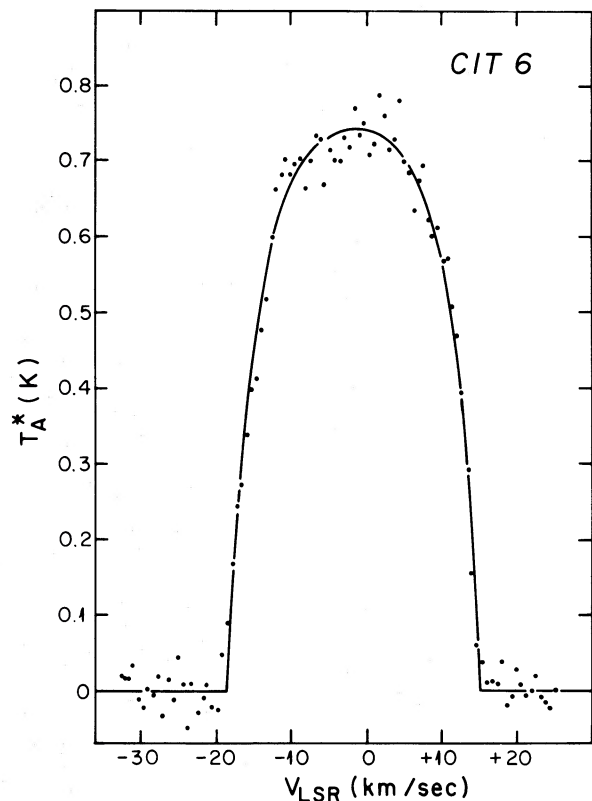


FIG. 3.—The CO(1-0) line profile of CIT 6. The fitted curve is a flattened parabola (see text).

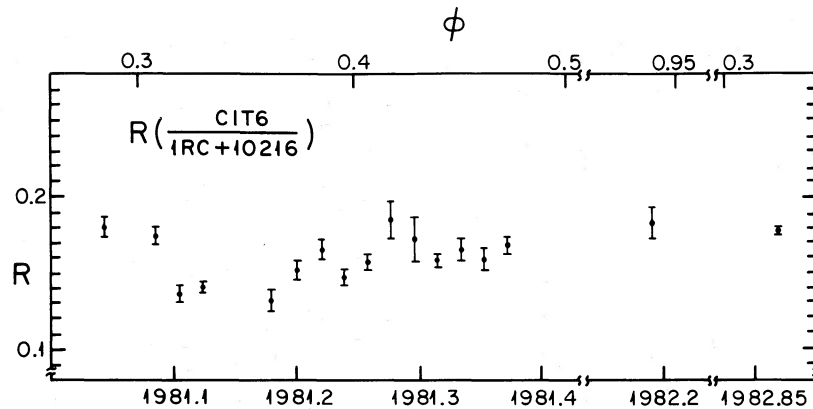


FIG. 4.—Time dependence of the integrated line intensity of CIT 6 (relative to that of IRC + 10216). The phase of the stellar variation (relative to maximum light) is given on the top horizontal axis.

(1982). The value of V_o , 15.2 km s^{-1} , is larger than the values of $14\text{--}14.5 \text{ km s}^{-1}$ found by these authors, but agrees with the value found by Kuiper *et al.* (1976).

d) Monitoring of CIT 6

At sufficiently low values of the mass loss rate and/or relative CO abundance, the CO in circumstellar envelopes is excited primarily by infrared radiation from the central star. There thus exists the possibility of variations in the intensity of the CO emission, because of changes in the infrared output of the star due to its intrinsic variability and, possibly, to other episodic occurrences (Cohen 1980). CIT 6 is a star whose emission has been suspected of such variability; the evidence for this, and a model to account for the possibly variable emission, are discussed by Morris (1980).

As part of this series of observations, the CO emission from CIT 6 was monitored at intervals of about one week, weather permitting, during the winter of 1980/1981. Two further observations were made at the beginning and end of 1982. To avoid large spurious effects, due, for example, to weather conditions or bad telescope pointing, an observation of IRC + 10216 was made at the same time. In Figure 4 we show the results of these monitoring observations, plotted as the ratio of the integrated line intensity for the two objects. The error bars are calculated from internal errors (noise) only. The phase of the variations of CIT 6, relative to maximum light, is also shown in the figure, from the ephemeris given by Alksnis and Khozov (1975). Apart from a possible decrease in 1981.1–1981.2, no significant variation of the CO flux of CIT 6 is evident in the figure, and neither

was variation in the line shape found. This agrees with the results of monitoring observations by Knapp, Kuiper, and Zuckerman (1979).

e) The 115.4 GHz Line of SiC_2 in CIT 6

Among the several unidentified lines discussed by Rodriguez Kuiper *et al.* (1977) is one at 115.383 GHz found in IRC + 10216. This has recently been identified as due to SiC_2 by Thaddeus, Cummins, and Linke (1984). We summed the monitoring observations of IRC + 10216 and CIT 6 and examined this frequency range in the 1 MHz resolution spectra. The line profile for IRC + 10216 is shown in Figure 5. The pronounced asymmetry in the line shape described by Rodriguez Kuiper *et al.* (1977) may be present in the spectrum shown in Figure 5. (This asymmetry is not present in the spectrum given by Cummins, Morris, and Thaddeus 1980.) Interestingly, the asymmetry is in the opposite sense from the slight asymmetry seen in the CO line (e.g., Fig. 2). Cummins, Morris, and Thaddeus (1980) also find that the intensity of the 115.4 GHz line relative to that of the CO line is 0.040 measured with the NRAO 11 m antenna. This value is very similar to that measured by the 7 m antenna (Table 3), suggesting that CO and SiC_2 have a similar spatial distribution in the envelope of IRC + 10216.

In Figure 6 we show the same spectral region for the summed data for CIT 6; the line is marginally detected. Its strength relative to the CO line is similar to that of IRC + 10216, as summarized in Table 3, consistent with the many other similarities of these two stars (e.g., Henkel *et al.* 1985).

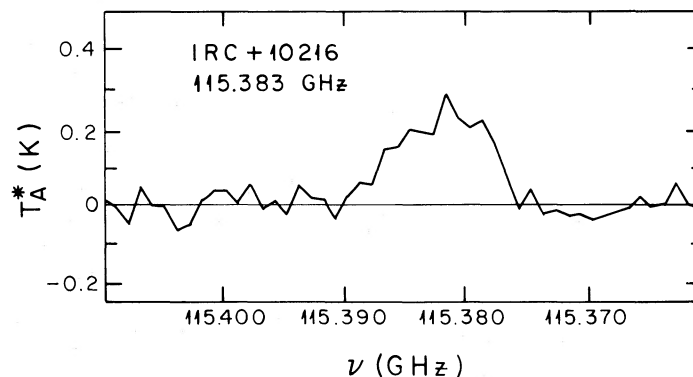


FIG. 5.—Profile of the SiC_2 (115.4 GHz) line for IRC + 10216, observed with a frequency resolution of 1 MHz .

TABLE 3
OBSERVATIONS OF THE SiC₂ LINE IN IRC +10216 AND CIT 6

Parameter	IRC +10216	CIT 6
Line intensity (K km s ⁻¹)	5.7 ± 0.6	0.70 ± 0.06
SiC ₂ /CO	0.046 ± 0.005	0.035 ± 0.003

III. MODELS OF CIRCUMSTELLAR ENVELOPE EMISSION

a) Qualitative Behavior of Models

In principle, the circumstellar envelopes represent a straightforward group of objects to be modeled; the velocity field, density distribution, and radiation field are all reasonably well known if there have not been strong variations in the mass loss rate. Calculations of the expected emission for various molecules have been made by Kwan and Hill (1977), Morris and Alcock (1977), Morris (1980), and Kwan and Linke (1982).

The special case of CO emission from circumstellar clouds presents some unique complications and difficulties. Other molecular species in circumstellar envelopes, less abundant than CO and with larger permanent dipole moments, are excited primarily by infrared radiation from the central star (with the possible exception of HCN; Jura 1983a). For CO, the infrared radiation competes with rotational excitation by collisions and by trapped rotational line photons to determine the populations of the rotational levels. This not only makes the coupled equations of level population and radiative transfer difficult to solve, but also has the result that there is no simple relationship between the envelope parameters and the observed emission which holds in all cases. Calculations by Morris (1980) indicate two well-defined regimes. When $\dot{M}f/V_o\Delta V \lesssim 0.7 \times 10^{-10}$, where \dot{M} is the mass loss rate in M_\odot yr⁻¹, f the abundance of CO relative to H₂, V_o the outflow velocity in km s⁻¹, and ΔV the local velocity dispersion due to the rms and turbulent broadening (km s⁻¹), the envelope is optically thin both tangentially in the rotational lines and radially in the $v = 0 \rightarrow 1$ line at 4.6 μ m, and infrared excitation dominates. In this case, Morris finds for a limited range of parameters, and for resolved envelopes,

$$T_A^\dagger(\text{line center}) \sim T_0 f \dot{M} D^{-1.2} V_o^{-2} \quad (3)$$

for the CO(1-0) line, where T_0 is weakly dependent on the infrared radiation field of the star, and D is the distance to the star. (Throughout this paper we denote antenna temperatures calculated from models by T_A^\dagger .)

The distance dependence in equation (3) arises because of the large outer radius of the model envelope, 5×10^{17} cm. At distances less than about 1 kpc, such envelopes are partially resolved. The resulting line profile is flat if $D \gtrsim 1$ kpc and becomes double-peaked at smaller distances. In general, Morris's models show that for optically thin envelopes it is difficult to avoid double-peaked profiles unless the effective envelope radius is small or the distance large.

For envelopes in which $\dot{M}f/V_o\Delta V \gtrsim 1.3 \times 10^{-10}$, Morris (1980) shows that the CO opacity exceeds unity for both the $v = 1 \rightarrow 0$, $J = 1 \rightarrow 0$ line at 4.6 μ m (radially) and, throughout much of the envelope, in the 2.6 mm $J = 1 \rightarrow 0$ line (tangentially). In this case, the resulting line profiles are rounded or parabolic. The profiles become increasingly flat-topped as the envelope becomes more resolved, IRC +10216 being a case in point. For optically thick envelopes with constant outflow velocities, the infrared field is relatively unimportant, and the level populations are dominated by collisions and radiative trapping of rotational line photons. Of course, a substantial radial velocity gradient, or an abrupt velocity shift in the outflow, would enhance the importance of IR excitation. Indeed, observations of multiple outflowing shells in some stars suggest that such an effect should ultimately be taken into account. In any case, the intensity of the CO line increases with \dot{M} , if f is held constant and if the radial temperature distribution is assumed not to depend on \dot{M} .

b) Input Data for Models of Circumstellar Envelope CO Emission

The above summary forms a context in which the present set of observations can be examined to discover the required range of parameters for models of the emission. Useful information can be obtained from an examination of the profile shapes and, in principle, by a comparison between the $J = 1-0$ intensities observed with the Bell Laboratories 7 m antenna and the NRAO 11 m antenna, and the $J = 2-1$ intensities observed with the OVRO 10 m antenna (Paper I).

The line profiles accumulated during the present investigation are presented in Figure 24; from these, an estimate of the profile shape can be made for most objects. The signal-to-noise ratio of the observations is such, however, that we often cannot reliably determine whether a given profile is flat or rounded.

Some stars (R Lep, α Ori, R Leo, Y CVn, RT Vir, Vy 2-2, IRC +10365, R Aur, and IRC +40483) were not observed with sufficient sensitivity to define their profile shapes. A few profiles (those of CRL 482, T Dra, RU Vir, and W Aql) appear

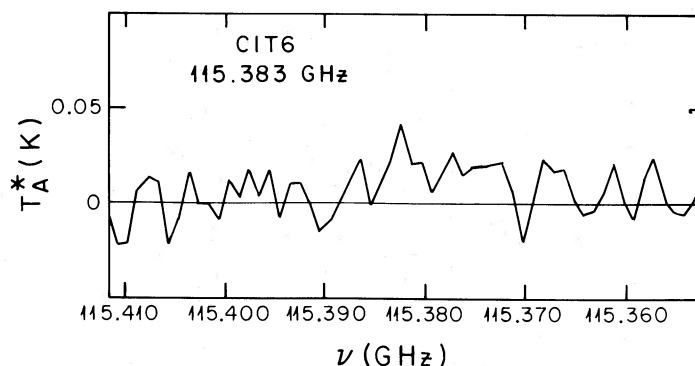


FIG. 6.—Spectrum near 115.4 GHz of CIT 6, observed with a frequency resolution of 1 MHz.

to be flat-topped. The profile of α Cet is Gaussian or triangular. The remaining line profiles are rounded. None of the line profiles shows any signs of being double-peaked, with the possible exceptions of those for R Scl, V Hya, and IRC +10365. This examination of the profile shapes suggests that many of the envelopes have optically thick CO emission.

In Table 4 we summarize the data for the detected stars, including the estimated distance to the star (col. [3]), and references for the distances (col. [4]). Many of these distances are

obtained by assuming that the bolometric luminosity of the star is $10^4 L_{\odot}$ (Smak 1966) and comparing this with the bolometric flux derived from infrared measurements. Interstellar extinction was ignored. The infrared data were taken from the extremely useful compilation by Gezari, Schmitz, and Mead (1982). Some of the distance estimates in Table 4 differ somewhat, though not greatly (except for χ Cyg), from those used in Paper I. The distance of Vy 2-2 is taken as 1 kpc to provide agreement between the CO line and the radio continuum

TABLE 4
DISTANCES AND ENVELOPE CHEMISTRY FOR EVOLVED STARS

Star (1)	Envelope Chemistry (2)	Distance (pc) (3)	Sources for Col. (3) (4)	T_A^* (NRAO) ^a (5)	R (6)	Spectrum (7)
IRC +40004	O	1100	1	0.21	0.45	M9
R And	S	309	2	0.26	0.51	S6e
IRC +10011	O	510	3	0.52	0.35	M
R Scl	C	840	1	0.69	0.45	C6 II
α Cet	O	77	4	1.12	0.34	M5e-M9e
CRL 482	C	1600	1	<0.38	...	C
IRC +50096	C	680	1	0.43	0.48	N
NML Tau	O	270	3	0.34	0.60	M6-10Me
IRC +60144	O	1000	1	M6
CRL 618	C	1300	5	0.60	0.72	PN, B0
IRC +60150	O	360	1	0.26	0.48	M9
R Lep	C	450	1	<0.46	...	N6e
IRC +50137	O	820	3	M10
R Aur	O	366	2	M7e-M9e
IRC +70066	O	800	1	≤ 0.15	...	M8
α Ori	O	400	6	<0.15	...	M2 Iab
CRL 865	C	1600	1	0.69	0.23	C
IRC +60169	O	750	1	≤ 0.15	...	M8
OH 231.8+4.2	O	1300	7	M6 I-M9 III
RS Cnc	O	410	1	0.31	0.32	M6 I-II
R Leo	O	304	2	<0.15	...	M7e-M9e
IRC +10216	C	290	8	7.5	0.68	C9, 5
CIT 6	C	190	9	0.95	0.78	C4, 3
IRC -10236	C	950	1	0.29	0.70	C
V Hya	C	400	1	0.52	0.44	C6, 3e
Y CVn	C	350	1	<0.38	...	C5, 4
RU Vir	C	1470	1	<0.38	...	R3ep
RT Vir	O	697	2	M8
RX Boo	O	225	1	M7-M8e
IRC +20326	C	1200	1	0.69	0.34	C
T Dra	C	525	2	<0.23	...	N0e (C8e)
CRL 2155	C	1330	1	0.34	0.52	C
CRL 2199	C	2000	1	0.34	0.47	C
IRC +10365	O	500	3	0.17	0.74	M9
IRC +20370	C	790	1, 9	0.86	0.37	C7, 3e
W Aql	S	470	1	0.69	0.52	S3, 9e-4, 9e
Vy 2-2	O	1000	10	PN
IRC +10420	O	3400	11	F8 Ia
χ Cyg	S	390	1, 6	0.52	0.55	S7 Ie:S10Ie
IRC -10529	O	620	3	0.26	1.17	M
V Cyg	C	510	2	0.78	0.48	C7, 4e
CRL 2688	C	1000	12	1.72	0.74	F5 Ia
IRC +00499	C	900	1	Ne, C
NGC 7027	C	1000	13	1.7	0.58	PN
IRC +40483	O	1100	3	M9
IRC +40485	C	780	1	0.43	0.27	C
CRL 3068	C	570	9	0.95	0.37	C
CRL 3099	C	500	1	<0.31	...	C
IRC +40540	C	960	9	0.95	0.49	C8, 3,4
R Cas	O	216	2	0.21	0.57	M6e-M9e

^a The symbol \lesssim denotes tentative detection.

SOURCES FOR COL. (3).—(1) Calculated from bolometric flux, assuming $L = 10^4 L_{\odot}$. (2) Bowers and Hagen 1984, or using Bowers and Hagen's $P-L$ relationship. (3) Hyland *et al.* 1972. (4) Allen 1973. (5) Westbrook *et al.* 1975. (6) See text. (7) Bowers and Morris 1984. (8) Herbig and Zappala 1970. (9) From Cohen 1979, or using Cohen's luminosity-spectral class relationships. (10) Distance unknown; 1 kpc assumed (see text). (11) Bowers, Johnston, and Spencer 1981. (12) Distance unknown; $D = 1$ kpc used by Ney *et al.* 1975. (13) Pottasch *et al.* 1982.

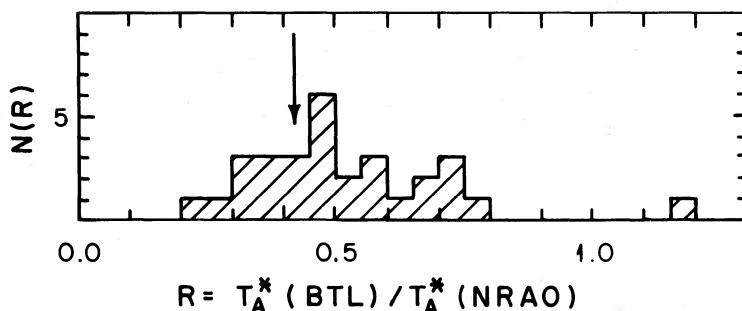


FIG. 7.—Distribution of the ratio of the T_A^* observed with the Bell Laboratories and NRAO telescopes for circumstellar envelopes. The value expected for an unresolved source, 0.42, is indicated by the arrow.

observations—this will be discussed in § IV. These distance estimates are in general very crude, but the kinematics of this group of objects shows that, statistically at least, the distance scale is reasonable (Knapp 1983).

Table 4 also lists the dominant envelope chemistry (col. [2]) and, where known, the spectral type of the star (col. [7]). The peak CO(1–0) temperature of the star measured with the NRAO 11 m telescope is given, when available, in column (5). These values are taken from the references given in the previous section and corrected where appropriate as described in Paper I. Column (6) gives the ratio R of the T_A^* values measured with the 7 m and 11 m antennas.

The distribution of R is shown in Figure 7. For a source of angular size much less than the beamwidth of either the 7 m or the 11 m telescope, R is expected to have the value 0.42, the square of the ratio of the half-power telescope beamwidths. Figure 7 illustrates the large observational scatter in this ratio, but also suggests that *most of the envelopes are unresolved by either the 7 m or the 11 m telescope*. The exceptions appear to be NML Tau, CRL 618, IRC +10216, CIT 6, IRC –10236, CRL 2688, NGC 7027 (?), and IRC –10529. The distance estimates given in Table 4 show that these objects are generally nearby.

Six of the stars in the present study have also been observed in the CO(1–0) line with the 20 m telescope (with HPBW = 33") at the Onsala Space Observatory (Nyman, Sahai, and Wannier 1985). In Table 5 we summarize the observations of these stars with the Bell Laboratories, NRAO, and Onsala telescopes. We give the ratio $T_A^*(\text{BTL}):T_A^*(\text{NRAO}):T_A^*(\text{OSO})$ expected for a point source, and calculated for each of the observed sources. Assuming that the CO emission does not vary, these observations suggest that CRL 618, χ Cyg, and NGC 7027 are essentially unresolved by our observations with the Bell Laboratories 7 m telescope, while CIT 6 and CRL 2688 are partially resolved, and are certainly resolved with the

Onsala 20 m telescope. The large uncertainties in the observational data are also very apparent.

The above qualitative discussion thus places two constraints on the models to be examined; many of the envelopes appear to be optically thick, and most of them are unresolved. A series of such models of the CO(1–0) emission is described immediately below.

c) Description of the Numerical Computations

The model for CO emission assumes a spherically symmetric envelope expanding at constant velocity. The local approximation is made in the excitation and radiative transfer calculations (following Kwan and Hill 1977 and using the formalism of Castor 1970), so that the level populations are independently calculated at each of 30 logarithmically spaced radii. The processes contributing to the molecular excitation are (1) interaction with the 2.7 K microwave background, (2) locally transferred rotational and vibrational line radiation, (3) collisions with H_2 , and (4) infrared continuum radiation in the vibration-rotation lines emitted from the stellar photosphere and from heated dust near the central star. The equations were solved for the lowest 15 rotational levels. Cross sections for collisional excitation by H_2 were linearly interpolated at each temperature from values calculated by Chapman and Green (1977) and McKee *et al.* (1982).

This model differs from that of Morris (1980), in which the local approximation is not used and different radial zones interact radiatively. The treatment used here has the advantage of simplicity and computational economy, but suffers the disadvantage that the local approximation gives a poor accounting of radially streaming radiation, such as the infrared radiation arising near the central star, when the outflowing matter has reached its terminal velocity and the radial velocity gradient is essentially zero [we have assumed that $V(r) \propto (1 - 4 \times 10^{14} \text{ cm } r^{-1})^{1/2}$, which is essentially constant in the region of interest, 10^{16} – 10^{18} cm]. Fortunately, for CO the vibrational lines become optically thick in the radial direction when the mass loss rate is greater than or about equal to the value at which collisional excitation dominates the excitation throughout the envelope. Therefore, IR excitation is important only when the vibration-rotation lines are optically thin, in which case the use of the local approximation in computing the radially streaming IR flux does not introduce a significant error.

The kinetic temperature profile within the envelope was assumed in all cases to be that derived by Kwan and Linke (1982) for IRC +10216. In principle, the heating and cooling at any point in the envelope depend on the physical character-

TABLE 5
RATIOS OF TEMPERATURES OBSERVED

Star	$T_A^*(\text{BTL})$	$T_A^*(\text{NRAO})$	$T_A^*(\text{OSO})$
Point source	1	2.37	9.18
CRL 618	1	1.40	6.74
CIT 6	1	1.28	2.43
χ Cyg	1	1.72	5.17
V Cyg	1	2.11	3.78
CRL 2688	1	1.31	3.15
NGC 7027	1	1.74	5.71

NOTE.—BTL: Bell Laboratories 7 m telescope; NRAO: NRAO 11 m telescope; OSO: Onsala 20 m telescope.

istics of the outflow (see, e.g., Tielens 1983), but since several of the input parameters in the temperature calculation are very uncertain, we choose not to attempt a self-consistent temperature determination. For the optically thick envelopes, our assumption of a universal temperature profile introduces some uncertainty into our suggested values for the CO loss rate (perhaps as much as a factor of 2), but they should not be too badly determined, since the temperature should change only weakly with \dot{M} and V_o (assuming that \dot{M} is proportional to luminosity) unless grain properties vary strongly with these parameters. In optically thin envelopes, on the other hand, the CO is excited primarily by IR radiation, and the kinetic temperature distribution plays an insignificant role.

Other details of the excitation calculations are similar to those described by Morris, Lucas, and Omont (1985). The calculations of profile shapes and intensities were carried out as described by Morris (1975). The model profiles depend on the distance D to the object (here measured in pc), the terminal outflow velocity V_o , the mass loss rate \dot{M} (here measured in $M_\odot \text{ yr}^{-1}$), the relative CO abundance $f = [\text{CO}]/[\text{H}_2]$, the maximum extent of CO molecules in the envelope, r_m (here measured in cm); and weakly upon the local line width ΔV (see Morris 1980). The dependence of the resulting emission on each of these quantities (except ΔV) was examined separately. For all of the computations except those in § III d [iv] a value $r_m = 3 \times 10^{17}$ cm was used, and for all of the calculations in this paper except those for the models of VY 2-2 and NGC 7027 the inner envelope radius was assumed to be 10^{15} cm.

d) Optically Thick Envelopes

i) Dependence on Distance D

Models were computed for distances in the range from 50 pc to 4 kpc. An example is shown in Figure 8, where the temperatures seen by the Bell Laboratories and NRAO antennas,

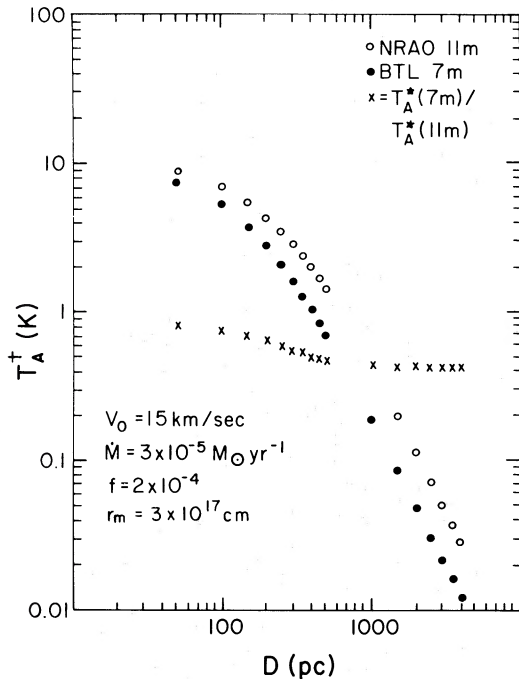


FIG. 8.—Values of the peak CO(1-0) line temperature T_A^\dagger for a model circumstellar envelope versus distance D for the 7 m and 11 m telescopes. The ratio of the line temperatures as a function of distance is also given.

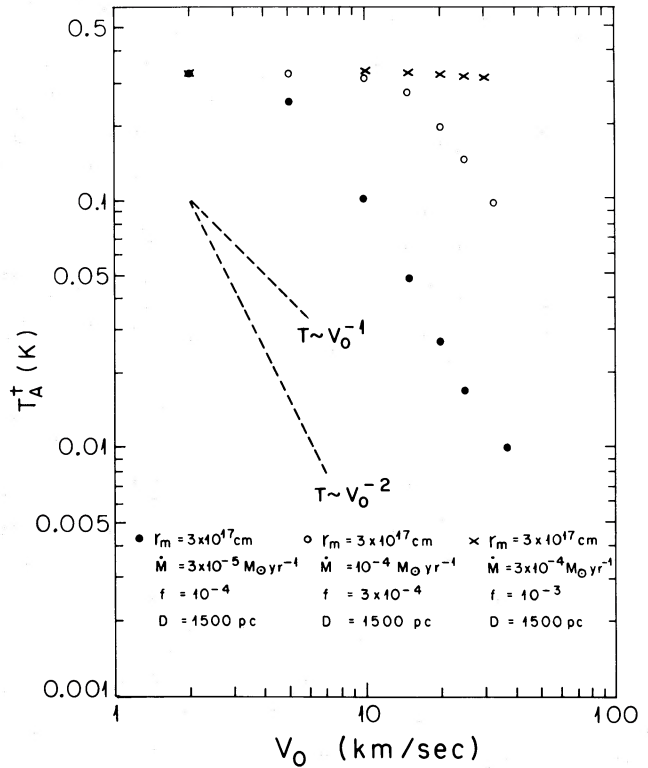


FIG. 9.—Three examples of the variation of T_A^\dagger with outflow velocity V_o . The shapes of the dependences $T_A^\dagger \propto V_o^{-1}$ and $T_A^\dagger \propto V_o^{-2}$ are indicated by the dashed lines.

and the temperature ratio, are plotted. The ratio shows the behavior discussed above; $R \rightarrow 0.42$ as $D \rightarrow \infty$. Closer than about 1 kpc, the envelope begins to be resolved. Since the observed values of R (Table 4; Fig. 7) suggest that most of the envelopes are unresolved, we adopt the distance dependence $T_A^\dagger \propto D^{-2}$. To avoid confusion by resolution effects, the following parameter investigations were carried out for $D = 1500$ pc, for the Bell Laboratories 7 m telescope.

ii) Dependence on Outflow Velocity V_o

The computations were carried out for a variety of models, with $D = 1500$ pc and $r_m = 3 \times 10^{17}$ cm, and a sample is shown in Figure 9. Figure 9 shows that the dependence on V_o falls into two regimes: (i) the envelope is extremely optically thick (here T_A^\dagger does not depend on any of the parameters of the envelope except r_m) and (ii) $T_A^\dagger \sim V_o^{-2}$ (e.g., Morris 1980). In the intermediate region, $T_A^\dagger \sim V_o^{-1}$ (e.g., Paper I). In Figure 10 we show a histogram of the observed values of V_o from Table 1; it can be seen that most of the observed velocities are $> 10 \text{ km s}^{-1}$. In addition, the product $f\dot{M}$ is $\lesssim 3 \times 10^{-8}$ for most envelopes (see below), so that the opacity is low enough to ensure that $T_A^\dagger \sim V_o^{-2}$.

iii) Dependence on Mass Loss Rate \dot{M} and CO Abundance f

Examples of the dependence of T_A^\dagger on \dot{M} and on f are given in Figures 11 and 12. T_A^\dagger rises almost linearly with both quantities, and begins to saturate when $\dot{M}f$ exceeds 10^{-8} . In Figure 13, T_A^\dagger is shown plotted against $\dot{M}f$, and is seen to rise slightly more slowly with f than with \dot{M} . T_A^\dagger rises more slowly than linearly with f because of partial saturation in the microwave lines, but the importance of saturation as \dot{M} increases is offset by the increase of collisional excitation in the outer envelope as

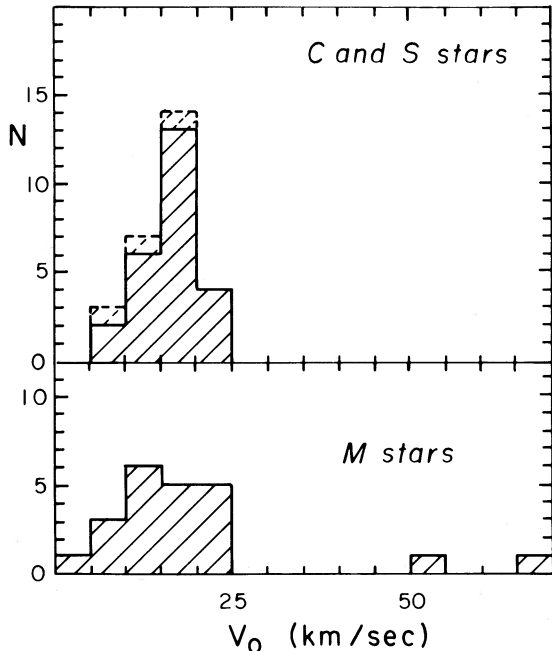


FIG. 10

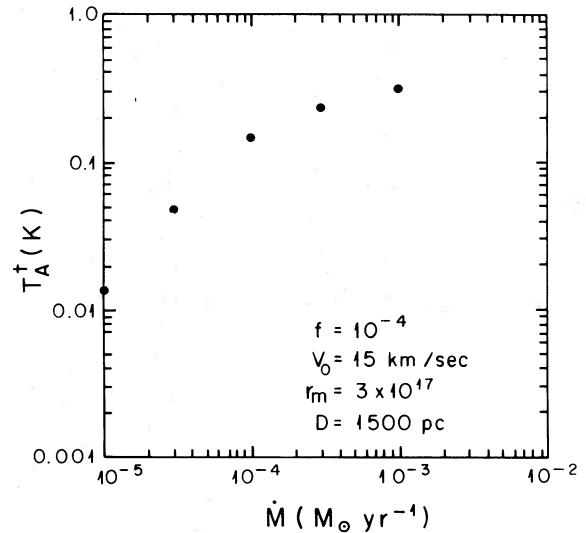


FIG. 11

FIG. 10.—Distribution of the outflow velocities V_0 observed via the CO(1–0) line for the stars in Table 1. In the upper panel, the values for the S stars are indicated by dashed lines.

FIG. 11.—Example of the dependence of $T_A^†$ on \dot{M} for a model circumstellar envelope

the density increases with larger \dot{M} (e.g., Paper I). For the range of interest, $3 \times 10^{-5} \lesssim f \lesssim 10^{-3}$, we find that $T_A^† \sim f^{0.85}$. This correspondence is illustrated in Figure 14, where we plot $T_A^†$ versus $\dot{M}f^{0.85}V_0^{-2}$ for a series of different calculations. Thus, in the range $5 \times 10^{-12} \lesssim \dot{M}f^{0.85}/V_0^2 \lesssim 6 \times 10^{-11}$, the temperature of the CO line at the systemic velocity of the star is given by

$$T_A^* \sim 0.047 \left(\frac{D}{1500 \text{ pc}} \right)^{-2} \left(\frac{\dot{M}}{3 \times 10^{-5} M_\odot \text{ yr}^{-1}} \right) \left(\frac{f}{10^{-4}} \right)^{0.85} \times \left(\frac{V_0}{15 \text{ km s}^{-1}} \right)^{-2} \quad (4)$$

($r_m = 3 \times 10^{17}$ cm). This relationship is also shown in Figure

14. For larger values of $\dot{M}f^{0.85}V_0^{-2}$ the temperature saturates (Fig. 14), although equation (4) is still accurate to $\sim 30\%$. Equation (4) shows that, if D and f are known, \dot{M} can be found from observations of the CO(1–0) line.

In Figure 15 are shown histograms of the quantity $T_A^*V_0^2D^2$, which, according to equation (4), should be roughly proportional to $\dot{M}f$. These histograms suggest that the mean value of $\dot{M}f$ tends to be higher for carbon stars than for oxygen-rich stars, which could be accounted for in part by the larger expected value of f for carbon stars (Fujita and Tsuji 1977). However, the distribution functions may differ as well; although both types of object exhibit the same overall range of mass loss rates, the distribution of $f\dot{M}$ in carbon stars appears to be substantially peaked at relatively larger values of $f\dot{M}$, whereas it is apparently flat for oxygen-rich stars.

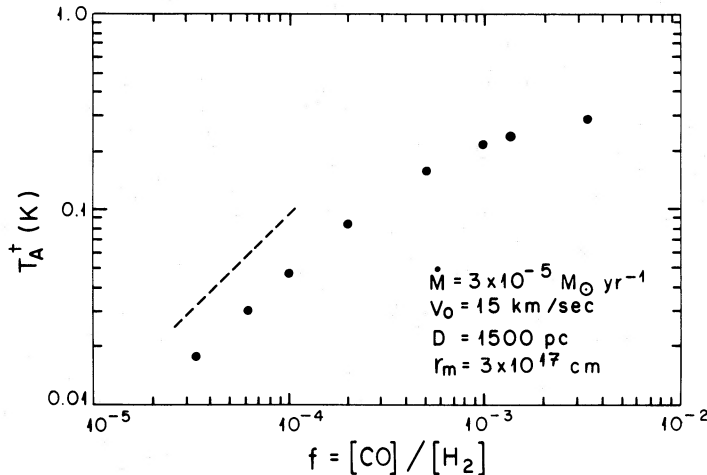


FIG. 12.—Example of the dependence of $T_A^†$ on fractional CO abundance, $f = [\text{CO}]/[\text{H}_2]$, for a model circumstellar envelope. The dependence $T_A^† \propto f$ is indicated by the dashed line.

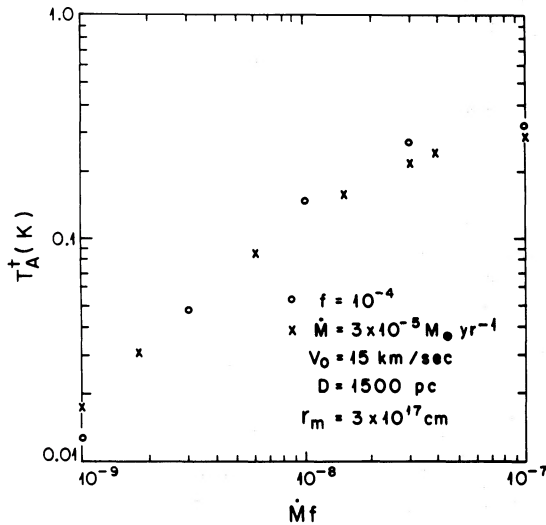


FIG. 13.—Dependence of T_A^\dagger on the product of the mass loss rate \dot{M} and the relative CO abundance f for two model circumstellar envelopes. For the models shown by circles, f was kept constant at 10^{-4} and \dot{M} was varied; for those indicated by crosses, \dot{M} was kept constant at $3 \times 10^{-5} M_\odot \text{ yr}^{-1}$ and f varied.

iv) Dependence on r_m

Finally, the dependence of T_A^\dagger on r_m was examined. The models used did not include the effects of dissociation by the interstellar radiation field; this will be discussed below. Because the effects of very large r_m were explored, the calculations were all done with a distance of 4 kpc to avoid possible resolution effects. Some examples of the calculations are shown in Figure 16. These calculations show that for $r_m \lesssim 10^{17}$ cm, T_A^\dagger is approximately proportional to the envelope area; then T_A^\dagger rises approximately linearly with r_m . However, for very large values of r_m the emissivity drops and T_A^\dagger levels off (Fig. 16). For a wide range of values of \dot{M} and f , the turnover occurs at values of r_m of a few $\times 10^{17}$ cm; at large radii, the density has dropped too low to collisionally excite the CO rotational levels above the excitation caused by the 2.7 K background. At such radii, each collision between a CO molecule and an H_2 molecule leads to the emission of a CO(1-0) photon, and $T_B(r) \sim r^{-3}$ (Jura 1984).

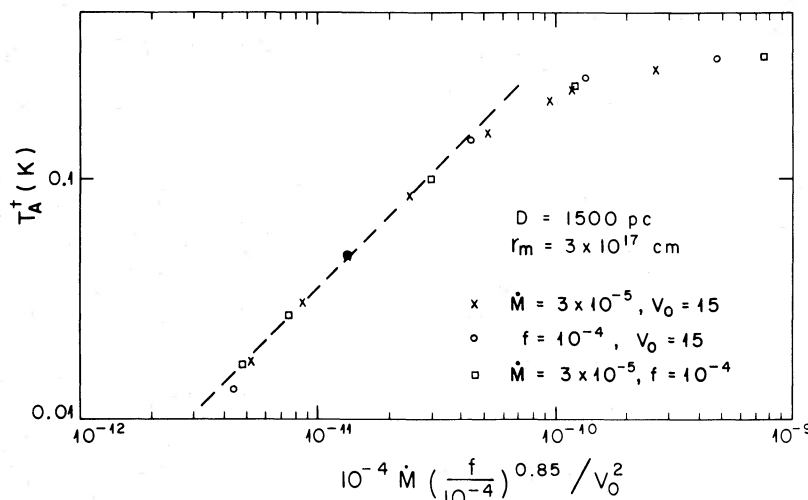


FIG. 14.—Dependence of T_A^\dagger on $10^{-4} \dot{M} (f/10^{-4})^{0.85} V_0^{-2}$ for several model circumstellar envelopes. The relationship corresponding to eq. (4) is shown by dashed lines.

v) Values of f

Figure 15 suggests that, if the mean value of \dot{M} does not depend on envelope chemistry, then the values of $f = [\text{CO}]/[\text{H}_2]$ are about 3 times higher for carbon stars than for oxygen stars. For solar abundances (Allen 1973), we expect $f = 6.6 \times 10^{-4}$ for oxygen Mira variables if all the C is in CO, while for carbon stars we expect $f = 1.3 \times 10^{-3}$ if all the O is in CO. However, the molecular abundances are poorly known, and the CO abundances may be strongly affected by the formation of dust. Here, we arbitrarily assume $f = 3 \times 10^{-4}$ for the oxygen Mira variables and 8×10^{-4} for the carbon stars (but see Kwan and Linke 1982). Values of \dot{M} for other assumed values of f can be obtained using equation (4).

vi) The Values of \dot{M}

The values of \dot{M} for the envelopes in Table 1 were calculated as follows. From the values of T_A^\dagger , V_0 , and D in Tables 1 and 4, an approximate value of $\dot{M}f$ was found from equation (4). If this value is such that $\dot{M}f/V_0 \gtrsim 1.3 \times 10^{-10}$ (Morris 1980), the envelope could be presumed to be optically thick in the CO lines; however, infrared excitation from the central star was included for both the optically thick and the optically thin envelopes. As expected, this makes a negligible difference for the optically thick envelopes; its effect for optically thin envelopes will be discussed below.

Equation (4) can be rearranged to give

$$\dot{M} = \frac{T_A^\dagger V_0^2 D^2}{2.0 \times 10^{15} f^{0.85}} M_\odot \text{ yr}^{-1}, \quad (5)$$

where D is in pc and V_0 in km sec, for $r_m = 3 \times 10^{17}$ cm. For $r_m = 10^{18}$ cm, the constant in the denominator becomes 2.1×10^{15} .

In the following computations, r_m was assumed to be either 10^{18} cm or r_c , whichever is smaller. The quantity r_c is the radius at which the flow rate of CO molecules is approximately equal to the photon flux of CO-dissociating interstellar ultraviolet radiation. If we assume that line dissociation dominates, Morris and Jura's (1983) equation (14) (with $L = 2$) becomes

$$r_c = 5.0 \times 10^{22} \left(\frac{\dot{M}f}{V_0} \right)^{1/2} \text{ cm}, \quad (6)$$

where \dot{M} is in $M_\odot \text{ yr}^{-1}$ and V_0 is in km s^{-1} .

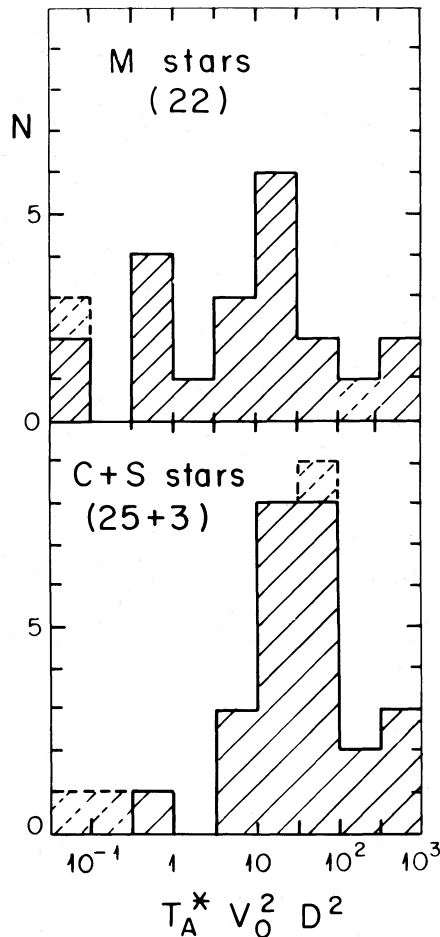


FIG. 15.—Histogram of the values of $T_A^* V_0^2 D^2$ (approximately proportional to $\dot{M}f$) from the quantities in Tables 1 and 4. In the upper panel is the histogram for oxygen stars; the two doubtful detections (α Ori and Vy 2-2) are indicated by dashed lines. In the lower panel is the histogram for carbon stars, with the S stars indicated by dashed lines.

e) Models for Individual Optically Thick Envelopes

Models were calculated for each of the stars whose envelope was found to be optically thick in the CO(1-0) line. For each envelope the value of \dot{M} was estimated from equation (5) and the parameters given in Tables 1 and 4, and was used in constructing a numerical model to give T_A^* for the 7 m telescope. The value of \dot{M} was then adjusted if necessary to give as close a fit as possible to $T_A^*(1-0)$. Equation (5) gives values of \dot{M} accurate to $\sim 20\%$ (if D , V_0 , and f are perfectly known), except for cases in which the CO is very optically thick or where the envelope is highly resolved (e.g., IRC + 10216). Also, for each fit, a profile was calculated to make sure that it agreed with the observed line shape. The fit was made in each case to the 7 m observation, but the values of $T_A^*(1-0)$ expected for the NRAO telescope and $T_A^*(2-1)$ for the OVRO 10 m telescope were also calculated. The calculated CO(2-1) temperatures, and a comparison with the observations of Paper I, are summarized in Table 8.

The results of the calculations for optically thick envelopes are given in Table 6, and are discussed below for some of the stars. The relevant observational information for each star from Tables 1 and 4 is summarized in Table 6, i.e., the peak CO line temperature as observed by the Bell Laboratories 7 m

telescope (col. [2]) and the outflow velocity (col. [3]). The assumed value of f is given in column (4). In column (5) is the value of \dot{M} found for each star, and in columns (6) and (7) the central CO(1-0) line temperature predicted from the model for the Bell Laboratories 7 m and NRAO 11 m telescopes, respectively. In column (8) is the value of \dot{M} corrected for the cosmic He, and in column (9) the critical radius r_c for CO photodissociation, calculated from equation (6). All of the values of r_c are close to or greater than 10^{18} cm. Thus, dissociation is not important for this group of objects unless the number of dissociating UV lines is substantially greater than 2, the number which we have assumed.

Model profiles for some of the individual stars, as observed with the 7 m and 11 m telescopes, are given as examples in Figure 17.

f) Optically Thin Envelopes

i) General Behavior of Models

For envelopes which are optically thin in the CO $v = 1-0$ line the effects of IR excitation must be included. The intensity and shape of the profile then depend on the IR flux, W (see below), as well as on V_0 , \dot{M} , f , and r_m . In this section we discuss the derivation of an approximate general formula relating the above physical parameters of the envelope to the observed CO $J = 1-0$ line intensity T_A^* , in the case where the IR lines are optically thin in the radial direction, as was done for optically thick envelopes in § III above. The formula of Morris (1980), quoted in equation (3) above, was modified because the objects studied in the present paper cover a wide range of distances, and also because the effect of photodissociation on limiting the effective envelope size must be taken into account. For all of the calculations described below except those in which the IR flux was varied, the $4.6 \mu\text{m}$ flux is taken to be that emitted by a blackbody of temperature 2000 K and radius 5×10^{13} cm (i.e., $W = 1$; Morris 1980), appropriately diluted.

ii) Dependence on Distance D

The observed values of $R = T_A^*(\text{BTL})/T_A^*(\text{NRAO})$ in Table 4 and Figure 7, as well as the Onsala observations (Table 5), suggest that many of the optically thin as well as optically thick

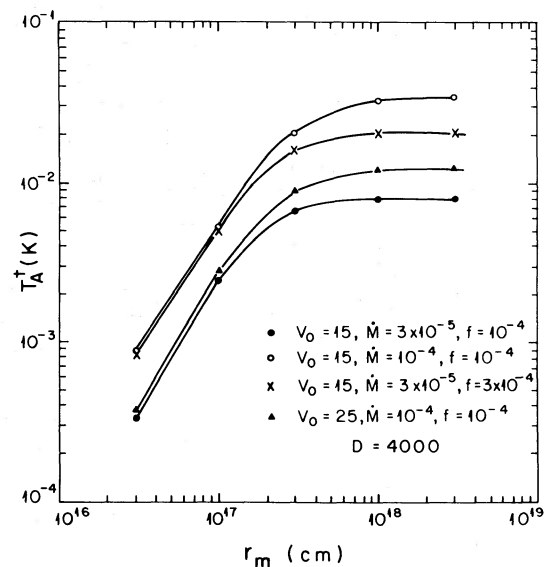


FIG. 16.—Examples of the dependence of T_A^* on the envelope radius r_m for several model circumstellar envelopes.

TABLE 6
MASS LOSS RATES FOR EVOLVED STARS WITH OPTICALLY THICK ENVELOPES

STAR (1)	T_A^* (BTL) (2)	V_o (km s ⁻¹) (3)	f (10 ⁻⁴) (4)	\dot{M} (M _⊙ yr ⁻¹) (5)	MODEL		\dot{M}_{corr} (M _⊙ yr ⁻¹) (8)	r_s^a (10 ¹⁶ cm) (9)
					T_A^* (BTL) (6)	T_A^* (NRAO) (7)		
IRC + 40004	0.09	24.2	3	2.4 × 10 ⁻⁵	0.09	0.20	2.7 × 10 ⁻⁵	0.86
IRC + 10011	0.18	23.0	3	1.2 × 10 ⁻⁵	0.18	0.37	1.4 × 10 ⁻⁵	0.63
R Scl	0.32	24.7	8	2.7 × 10 ⁻⁵	0.33	0.69	3.1 × 10 ⁻⁵	1.5
CRL 482	0.11	16.0	8	1.5 × 10 ⁻⁵	0.11	0.25	1.7 × 10 ⁻⁵	1.4
IRC + 50096	0.21	16.8	8	5.5 × 10 ⁻⁶	0.21	0.46	6.3 × 10 ⁻⁶	0.81
IRC + 60144	0.12	20.4	3	2.0 × 10 ⁻⁵	0.12	0.26	2.3 × 10 ⁻⁵	0.86
CRL 618	0.43	21.5	8	6.7 × 10 ⁻⁵	0.43	0.94	7.7 × 10 ⁻⁵	2.5
IRC + 70066	0.08	21.1	3	1.0 × 10 ⁻⁵	0.08	0.18	1.1 × 10 ⁻⁵	0.60
CRL 865	0.16	15.3	8	2.0 × 10 ⁻⁵	0.16	0.37	2.3 × 10 ⁻⁵	1.6
OH 231.8+4.2	0.04	68.5	3	1.1 × 10 ⁻⁴	0.04	0.09	1.3 × 10 ⁻⁴	1.1
IRC + 10216	5.10	15.2	8	4.8 × 10 ⁻⁵	5.10	8.00	5.5 × 10 ⁻⁵	2.5
IRC - 10236	0.21	10.9	8	4.1 × 10 ⁻⁶	0.21	0.46	4.7 × 10 ⁻⁶	0.87
V Hya	0.22	20.9	8	3.5 × 10 ⁻⁶	0.22	0.44	4.0 × 10 ⁻⁶	0.58
RU Vir	0.07	16.9	8	8.3 × 10 ⁻⁶	0.07	0.16	9.5 × 10 ⁻⁶	0.99
IRC + 20326	0.23	17.5	8	2.0 × 10 ⁻⁵	0.23	0.51	2.3 × 10 ⁻⁵	1.5
CRL 2155	0.18	15.1	8	1.5 × 10 ⁻⁵	0.18	0.40	1.7 × 10 ⁻⁵	1.4
CRL 2199	0.16	8.0	8	1.1 × 10 ⁻⁵	0.16	0.37	1.3 × 10 ⁻⁵	1.7
IRC + 20370	0.32	15.6	8	9.1 × 10 ⁻⁶	0.32	0.68	1.0 × 10 ⁻⁵	1.1
W Aql	0.36	19.9	6	8.6 × 10 ⁻⁶	0.36	0.74	9.8 × 10 ⁻⁶	0.87
IRC + 10420	0.03	51.7	3	2.6 × 10 ⁻⁴	0.03	0.07	3.0 × 10 ⁻⁴	1.9
IRC - 10529	0.30	15.8	3	1.3 × 10 ⁻⁵	0.29	0.61	1.5 × 10 ⁻⁵	0.79
CRL 2688	1.27	19.7	8	1.4 × 10 ⁻⁴	1.26	2.42	1.6 × 10 ⁻⁴	3.8
IRC + 00499	0.09	16.4	8	3.8 × 10 ⁻⁶	0.09	0.21	4.4 × 10 ⁻⁶	0.68
NGC 7027 ^b	0.98	17.9	8	9.7 × 10 ⁻⁵	0.98	1.87	1.1 × 10 ⁻⁴	3.3
CRL 3068	0.36	14.5	8	6.4 × 10 ⁻⁶	0.36	0.78	7.3 × 10 ⁻⁶	0.94
IRC + 40540	0.47	14.7	8	2.1 × 10 ⁻⁵	0.48	1.02	2.4 × 10 ⁻⁵	1.7

^a In col. (9) the mass loss rate corrected by 15% for the cosmic helium abundance (Allen 1973) is given.

^b Inner shell radius corresponding to planetary nebula radius used (see text).

envelopes are unresolved by the Bell Laboratories antenna. Thus the dependence of intensity on distance is $T_A^* \sim D^{-2}$. To avoid confusion by resolution effects, all of the calculations described below are made for a distance of 1500 pc.

iii) *Dependence on Wind Velocity V_o*

Since the line opacity τ is proportional to V_o^{-2} (Morris 1980), the antenna temperature should also be proportional to V_o^{-2} in the optically thin case. This is borne out by the models.

iv) *Dependence on $f = [\text{CO}]/[\text{H}_2]$*

A series of models showing the dependence on f over the range $(2-10) \times 10^{-4}$ is shown in Figure 18, demonstrating that $T_A^* \sim f$.

v) *Dependence on \dot{M}*

A set of models showing the dependence of T_A^* on \dot{M} is given in Figure 19; over a wide range of \dot{M} , $T_A^* \sim \dot{M}$. The effects of increasing opacity in the $v=1-0$ line at large f and \dot{M} can be seen in Figures 18 and 19.

vi) *Dependence on r_m*

A series of models showing the dependence of T_A^* on r_m is shown in Figure 20. Here r_m was varied independently of the value of $\dot{M}f/V_o$, which sets the radius at which CO dissociation takes place. Over an appropriate range of r_m , we find that $T_A^* \sim r_m^{0.4}$.

vii) *Dependence on W*

As will be seen below, the range of values of W for the observed stars is about 0.1-5, where W measures the ratio of the 4.6 μm flux to that of the "standard" 2000 K, 5×10^{13} cm

blackbody. The results for one set of models (Fig. 21) over this range of W indicate an approximately logarithmic dependence,

$$T_A^* \propto \log \left(\frac{W}{0.04} \right). \quad (7)$$

In the limited range of W considered, this logarithmic dependence does not differ greatly from the $W^{1/2}$ dependence suggested by Morris and Alcock (1977) for the intensities of the SiO rotational lines.

The calculations presented in Figures 17-21 yield

$$T_A^* = 3.7 \times 10^{-4} \log \left(\frac{W}{0.04} \right) \left(\frac{r_m}{4 \times 10^{17} \text{ cm}} \right)^{0.4} \left(\frac{D}{1500 \text{ pc}} \right)^{-2} \\ \times \left(\frac{\dot{M}}{10^{-7} M_{\odot} \text{ yr}^{-1}} \right) \left(\frac{f}{2 \times 10^{-4}} \right) \left(\frac{V_o}{15} \right)^{-2} \text{ (K)} \quad (8)$$

for the Bell Laboratories 7 m antenna, with about 30% accuracy over the range of parameters considered here. For the NRAO 11 m and Onsala 20 m telescopes, the numerical coefficients for equation (8) are $\sim 1.7 \times 10^{-3}$ and 5.9×10^{-3} , respectively. Equation (8) is not quite the final answer, because r_m depends on \dot{M} . If it is assumed that the envelopes are of arbitrarily large age, the value of r_m can be found using equation (6), since, for these optically thin envelopes, the radius at which CO is dissociated is of order several $\times 10^{17}$ cm. Thus, if D , W , V_o , and f are known, the combination of equations (6) and (8) can be used to find \dot{M} from the intensity of the CO(1-0) line. This was done for the individual optically thin envelopes, and the results are discussed below.

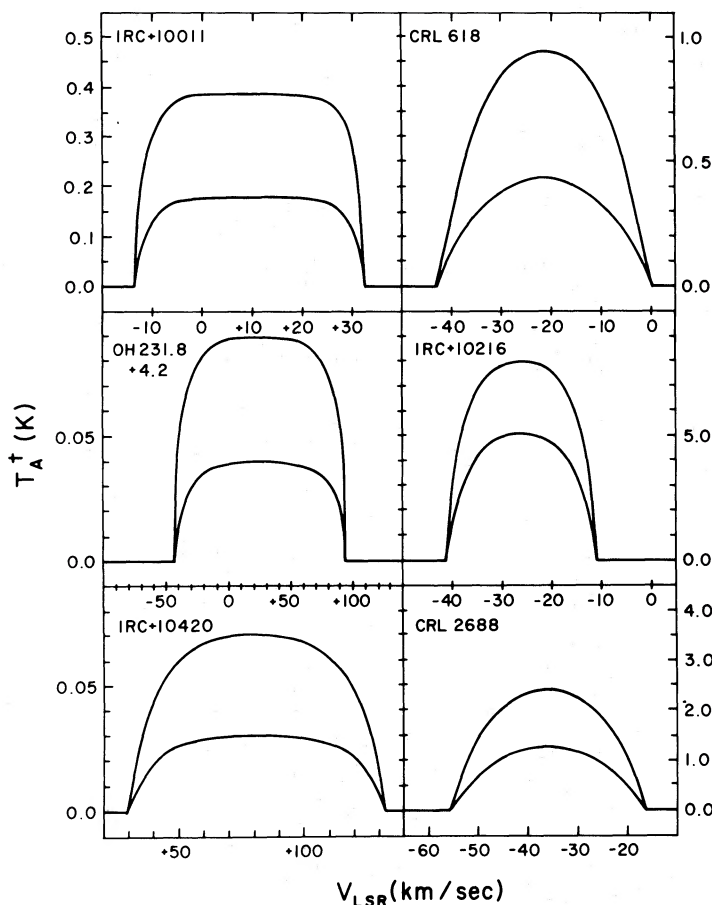


FIG. 17.—Examples of model CO(1-0) line profiles for six stars with optically thick envelopes, as observed with the NRAO 11 m (*upper curves*) and Bell Laboratories 7 m telescopes.

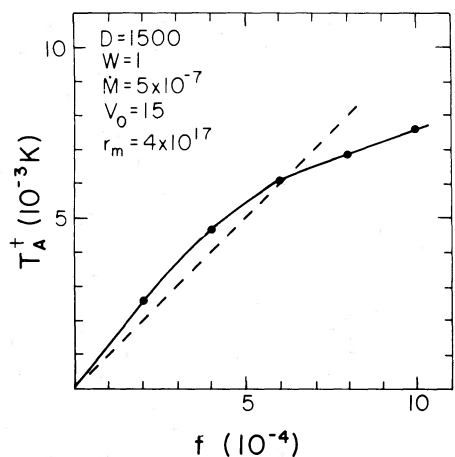


FIG. 18.—Dependence of T_A^+ on fractional CO abundance f for model optically thin envelopes. The dashed line is the relationship $T_A^+ \propto f$.

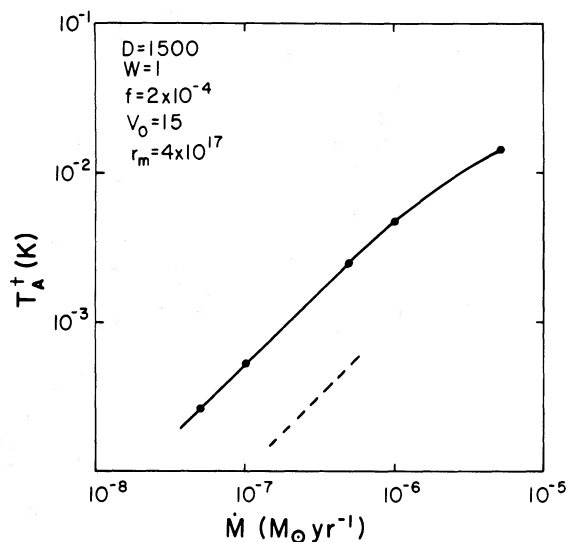


FIG. 19.—Dependence of T_A^+ on mass loss rate \dot{M} for model optically thin envelopes. The dashed line gives the slope of the relationship $T_A^+ \propto \dot{M}$.

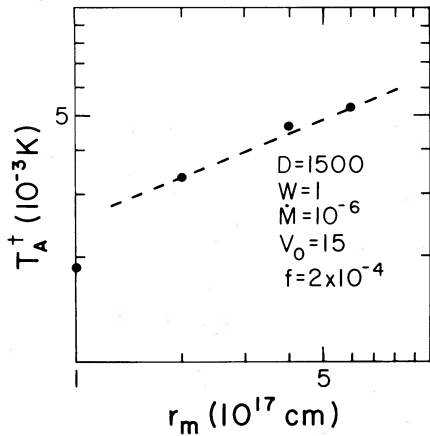


FIG. 20.—Dependence of T_A^\dagger on maximum envelope radius r_m for model optically thin envelopes. The dashed line has a slope corresponding to $T_A^\dagger \propto r_m^{0.4}$.

g) Models for Individual Optically Thin Envelopes

For each star, an approximate value of \dot{M} was found from equations (8) and (6), and then checked and adjusted by calculating a specific model to fit the data for each star. The values of the 4.6 μm flux were found from the compilation of Gezari, Schmitz, and Mead (1982). For variable stars, a mean value of the flux was used.

The results are given in Table 7, where we list (1) the star's name, (2) the assumed value of f , (3) T_A^\dagger measured with the 7 m telescope, (4) the IR flux in $\text{ergs cm}^{-2} \text{s}^{-1} \mu\text{m}^{-1}$ measured near 4.6 μm , (5) the wavelength of observation, (6) the reference for the IR photometry, and (7) the implied value of W . The results of the model fitting are in columns (8)–(12): \dot{M} , the computed values of T_A^\dagger for the 7 m and 11 m telescopes, and the profile shapes for the 7 m and 11 m telescopes. In column (13) is the value of r_c , the radius at which we estimate the CO to be dissociated, and in column (14) the value of \dot{M} corrected for the He content. For both the optically thick and the optically thin envelopes, the predicted values of $T_A^\dagger(2-1)$ which would be observed with the Owens Valley 10 m telescope were calculated. These are compared with the data in Table 8. The data are taken from Paper I, with the temperature scale adjusted for a half-power beamwidth of 30". Observations made separately

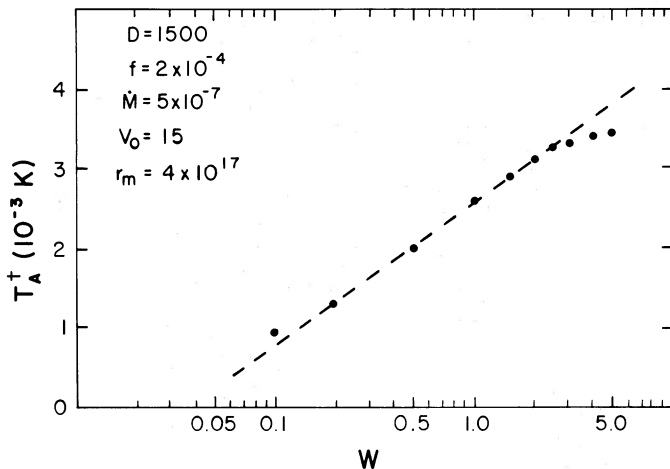


FIG. 21.—Dependence of T_A^\dagger on infrared flux W for model optically thin envelopes. The dashed line has a slope corresponding to $T_A^\dagger \propto \log(W/0.04)$.

of spectral line profiles or maps at the systemic stellar velocity (see Paper I) are listed separately. The agreement between the observations and the predictions is of the same order as the observational uncertainty.

IV. DISCUSSION

a) Uncertainties in the Derived Values of \dot{M} and Comparison with Previous Results

Equations (4), (6), and (8) show that the mass loss rates can be estimated from the CO observations using an equation like

$$\dot{M} = A(w, r_m) \frac{T_A^* V_0^2 D^2}{f},$$

where A is the numerical coefficient found from modeling. Some of the quantities are obtained from molecular line observations such as those discussed here; others, such as f , are estimates; and the values of distance D are taken from the literature.

By far the largest uncertainties are those in the distances. Since most of the distance estimates are quoted without error bars, it is impossible to make a realistic estimate of the errors in the resulting values of \dot{M} . In this section the case of each individual star will be discussed, and the various values of D compared. Several methods are used in the literature for estimating distances. These include the following:

1. The phase-lag–angular size comparison for OH masers (Booth, Diamond, and Norris 1984; Bowers, Johnston, and Spencer 1983). These should provide very reliable distance values, but are at present available for only a few stars, and in any case apply only to stars with OH maser emission.

2. The assumption that $L_{\text{bol}} = 10^4 L_\odot$ (e.g., Hyland *et al.* 1972; present paper). These distance estimates could be in error by a factor of 2.

3. Spectral type–luminosity relationships (Herbig and Zappala 1970; Cohen 1979); similar relationships are used by Rowan-Robinson and Harris (1982, 1983a, b, hereafter RH).

4. Period–absolute magnitude relationships (van den Bergh 1984; Celis 1981, 1984).

The application of these relationships in the visible range of the spectrum is very susceptible to large errors caused by interstellar and, especially, circumstellar extinction. Bowers and Hagen (1984) have found distances using these relationships and extinction models.

These errors in distances are sufficient to ensure that individual mass loss rates are usually uncertain by a factor of 10. Until much better distances are widely available, data such as the present compilation are best used in distance-independent studies, such as that of the total rate of return of mass to the interstellar medium, described in the next section.

The numerical coefficient $A(W, r_m)$ is probably known to about 50% from the modeling; the uncertainties arise because we have assumed a constant kinetic temperature gradient $T_k(r)$ for all stars. The dependence on W and r_m is relatively unimportant for high values of \dot{M} , while the dependence of $T_k(r)$ is relatively unimportant for low values of \dot{M} , where much of the excitation of the CO(1–0) line is due to infrared radiation. The assumed value of W is affected by the assumed distance; however, if D (hence W) is overestimated, \dot{M} will also be overestimated, and hence the effect of infrared radiation is lessened. Thus distance errors do not cause a significantly larger error due to miscalculation of W . The value of r_m is not well known because the effect of photodissociation of circumstellar CO is

TABLE 7
MASS LOSS RATES FOR STARS WITH OPTICALLY THIN ENVELOPES

Star (1)	Assumed f (10^{-4}) (2)	T^* (BTL) (3)	Flux ^a (4)	λ (flux) (μm) (5)	References (6)	W (7)	\dot{M} ($M_{\odot} \text{ yr}^{-1}$) (8)	T_A^1 (BTL) (9)	T_A^1 (NRAO) (10)	Profile (BTL) (11)	Profile (NRAO) (12)	r_c (10^{17} cm) (13)	\dot{M}_{corr}^b ($M_{\odot} \text{ yr}^{-1}$) (14)	Notes (15)
R And	6	0.13	8.3×10^{-8}	4.2	1	0.48	3.2×10^{-7}	0.13	0.27	F	F	2.3	3.7×10^{-7}	
α Cen	3	0.38	5.3×10^{-7}	4.9	2	0.30	5.7×10^{-7}	0.38	0.60	P	P	0.15	6.5×10^{-7}	1
NML Tau	3	0.20	1.7×10^{-7}	4.8	3	1.80	4.5×10^{-6}	0.20	0.38	F	F	3.9	5.1×10^{-6}	
IRC + 60150	3	0.12	1.5×10^{-7}	4.9	4	1.90	9.3×10^{-7}	0.12	0.25	F	F	2.4	1.1×10^{-6}	
R Lep	8	0.09	5.6×10^{-8}	4.9	5	1.10	1.8×10^{-6}	0.09	0.19	F	F	4.2	2.1×10^{-6}	
IRC + 50137	3	0.08	2.1×10^{-8}	4.2	1	0.93	5.7×10^{-6}	0.08	0.17	F	F	5.4	6.5×10^{-6}	
R Aur	3	0.06	1.2×10^{-7}	4.2	1	0.97	4.6×10^{-7}	0.06	0.14	F	F	1.8	5.3×10^{-7}	
α Ori	3	0.01	1.2×10^{-6}	4.9	5	4.63	1.2×10^{-6}	0.01	0.017	F	F	0.6	1.4×10^{-7}	2
IRC + 60169	3	0.08	5.7×10^{-8}	4.2	1	1.89	5.5×10^{-6}	0.08	0.17	R	F	4.9	6.3×10^{-6}	
RS Cnc	3	0.12	1.2×10^{-7}	4.9	5	2.01	2.5×10^{-7}	0.12	0.27	F	F	1.9	2.9×10^{-7}	
R Leo	3	0.05	5.1×10^{-7}	4.9	5	3.45	8.0×10^{-8}	0.05	0.11	P	P	1.2	9.2×10^{-8}	
CIT 6	8	0.74	3.8×10^{-7}	4.8	3	1.08	2.6×10^{-6}	0.74	1.35	F	F	5.5	3.0×10^{-6}	3
Y CVn	8	0.06	6.1×10^{-8}	4.9	5	0.75	9.0×10^{-8}	0.06	0.13	F	F	1.5	1.0×10^{-7}	4
RT Vir	3	0.08	1.6×10^{-7}	4.2	1	4.37	1.3×10^{-6}	0.08	0.17	F	F	2.9	1.5×10^{-6}	
RX Boo	3	0.09	1.9×10^{-7}	4.9	5	0.89	3.3×10^{-7}	0.09	0.17	F	P	1.5	3.8×10^{-7}	
T Dra	8	0.07	2.2×10^{-8}	4.8	6	0.54	1.1×10^{-6}	0.07	0.16	F	F	3.8	1.3×10^{-6}	
IRC + 10365	3	0.13	4.6×10^{-8}	4.9	4	0.89	5.5×10^{-6}	0.13	0.27	R	R	5.0	6.3×10^{-6}	
Vy 2-2	3	0.02	3.2×10^{-11}	4.2	1	0.003	2.1×10^{-6}	0.02	0.04	R	F	2.6	2.4×10^{-6}	5
χ Cyg	6	0.29	3.3×10^{-7}	4.9	2	3.90	1.5×10^{-6}	0.29	0.59	P	P	4.7	1.7×10^{-6}	
V Cyg	8	0.37	1.5×10^{-7}	4.9	2	3.90	3.0×10^{-6}	0.36	0.72	R	R	6.8	3.4×10^{-6}	6
IRC + 40483	3	0.04	1.4×10^{-8}	4.2	1	1.05	7.2×10^{-6}	0.04	0.09	F	F	5.5	8.2×10^{-6}	
IRC + 40485	8	0.11	6.6×10^{-8}	4.8	3	3.74	2.3×10^{-6}	0.11	0.24	R	R	5.6	2.6×10^{-6}	
CRL 3099	8	0.16	1.3×10^{-8}	4.2	1	0.30	1.3×10^{-6}	0.16	0.35	R	R	5.1	1.5×10^{-6}	
R Cas	3	0.12	3.0×10^{-7}	4.9	2	1.35	4.5×10^{-7}	0.12	0.21	P	P	1.6	5.1×10^{-7}	

NOTES.—(1) The profile shape was not fitted (see text). (2) T_A^* from total CO(1-0) flux in Table 1, divided by $\Delta V = 30 \text{ km s}^{-1}$. (3) CIT 6; the model predicts $T_A^*(\text{OSO}) = 3.2$; the observed value is 1.8 K. (4) Model stellar flux agrees with that of Goebel *et al.* 1980. (5) Vy 2-2; Inner shell radius corresponding to planetary nebula radius used (see text). (6) V Cyg: The model predicts $T_A^*(\text{OSO}) = 1.9$; the observed value is 1.4 K.

^a Units of $4.6 \mu\text{m}$ flux are $\text{ergs s}^{-1} \text{ cm}^{-2} \mu^{-1}$.

^b \dot{M}_{corr} is corrected by 15% for the cosmic helium abundance.

REFERENCES FOR IR Photometry.—(1) Price and Walker 1976; (2) Forrest, Gillett, and Stein 1975; (3) Strecker and Ney 1974; (4) Merrill and Stein 1976; (5) Gillett, Merrill, and Stein 1971; (6) Hackwell 1972.

TABLE 8

COMPARISON OF OBSERVED AND MODEL CO(2-1) INTENSITIES

STAR	$T_A^*(2-1)$		$T_A^*(2-1)$
	Spectrum	Map	
IRC +10011	1.6	2.3	1.2
<i>o</i> Cet	6.2	10.3	9.1, (2.0)
CRL 618	3.5	1.8	2.1
α Ori	1.1	1.2	0.5, (0.2)
CRL 865	1.9	1.3	1.0
RS Cnc	0.7	1.1
R Leo	0.6	0.5	0.8
IRC +10216	14.7	23.7	16.4
CIT 6	2.5	2.6	4.2
RX Boo	1.7	...	0.6
IRC +20370	1.9	...	1.8
χ Cyg	0.8	...	1.7
CRL 2688	1.9	4.5
NGC 7027	5.0	2.7
CRL 3068	2.1	1.7	2.3

NOTE.—Values of $T_A^*(2-1)$ are from Paper I, corrected to a beamwidth of 30".

little understood; the appropriate value of r_m can, however, be roughly calibrated using observations of IRC +10216 (cf. eq. [6]). In any case, the coefficient $A(W, r_m)$ is probably in error by $\sim 50\%$. In Paper I, values of \dot{M} were calculated with the effect of infrared radiation ignored; for stars with small values of \dot{M} , then, the values of \dot{M} in Paper I are likely to be overestimates.

We have no direct knowledge of the value of $f = [\text{CO}]/[\text{H}_2]$ in any individual case, and the values of \dot{M} are likely to be uncertain to about a factor of 2 because of uncertainties in the assumed values of f . The approximate formulae of Paper I do not take account of composition differences among stars; comparison with the present work shows that these formulae probably provide reasonably good values of \dot{M} for Mira variables, but overestimate \dot{M} for carbon and S stars.

Equations (4), (6), and (8) depend on the observed parameters of the CO line according to $\dot{M} \propto \sum T_A^* \Delta V \times V_0$. The integrated CO line intensity $\sum T_A^* \Delta V$ is measured to $\sim 20\%$ for the stronger lines and $\sim 50\%$ for the weaker lines, where the uncertainties are due to calibration errors and nonflat baselines. Likewise, errors in V_0 can be larger than the values quoted in Table 1 if there is low-level baseline ripple present. Also, as described in § II, the fitting procedure used in the present paper could overestimate V_0 if the line profile is flat rather than parabolic. Eye estimates of V_0 , found from the full width of the line at zero power, are difficult because of noise, and are likely to underestimate V_0 . In the following discussion of individual stars, the present estimates are compared with those previously published; however, much of the previous observational work on the CO(1-0) line has been presented in terms of ΔV , the full line width at half-power. If the line profile is parabolic, $V_0 = \Delta V \sqrt{2}$, while if it is flat-topped, $V_0 = \Delta V/2$. Since most of the previous work is presented with neither error estimates nor any information on profile shape, the resulting values of V_0 are very uncertain. References to previous CO(1-0) observations are given in Paper I.

Overall, the uncertainties in the values of \dot{M} listed in Tables 6 and 7 are about a factor of 1.5-3, in addition to distance uncertainties, which give an additional factor of 2-10. The values of \dot{M} found in the present paper are somewhat higher than those of Morris (1980) because we have included the effect of interstellar ultraviolet light in truncating the effective

envelope radius. In this last context, it is now clear that the observational fact that resolved envelopes are rarely seen (either by their expected double-peaked line profiles or by the relative intensities seen by telescopes of different sizes) is due to this dissociative truncation of the CO envelope. The individual stars are now discussed.

IRC +40004.—The observations of the CO(1-0) line reported here and by Zuckerman (1981) are in good agreement. However, the distance estimate in Table 4 (1100 pc) differs from that of RH, who find a value of 700 pc.

R And.—The value of \dot{M} listed in Table 7 is a factor of 6 lower than that in Paper I. This is partly due to the neglect of IR excitation in Paper I, but most of the effect is due to the lower value of V_0 measured here—the value of V_0 in Paper I, taken from a measurement of ΔV by Lo and Bechis (1977), was probably overestimated, as discussed above.

IRC +10011.—Model profiles for this object are given in Figure 17. If we assume that $f = 3 \times 10^{-4}$, a fit to the 7 m data alone gives $\dot{M} = 1.4 \times 10^{-5} M_\odot \text{ yr}^{-1}$, close to the value of $2 \times 10^{-5} M_\odot \text{ yr}^{-1}$ found using measurements of the linear size of the OH maser-emitting region (Bowers, Johnston, and Spencer 1983; Booth, Diamond, and Norris 1984), but smaller than the value of $5 \times 10^{-5} M_\odot \text{ yr}^{-1}$ found by Jura (1983b) from the mapping data of Paper I or the value of 2.6×10^{-5} given in Paper I. The predicted values of T_A^* for both the NRAO CO(1-0) and the OVRO CO(2-1) data are somewhat lower than the observed values, suggesting that the mass loss rate may be as much as twice as high for this star as the value given in Table 6. The values of V_0 given in the literature are in reasonable agreement with that in Table 1. RH estimate the star's distance to be 1200 pc, although the OH measurements support the value of 510 pc used here (Booth, Diamond, and Norris 1984).

R Scl.—The value of V_0 in Table 1 is much larger than the value of 16 km s⁻¹ quoted in Paper I; data with a better signal-to-noise ratio are needed for an adequate measurement of V_0 . The period- M_v relationship of van den Bergh (1984) suggests $D = 910$ pc, in reasonable agreement with the value derived here of 840 pc, but RH suggest $D = 400$ pc.

o Cet.—A first attempt was made to fit the CO(1-0) line intensity for this star, using equation (6) to define the outer envelope radius. The resulting fit was very poor; the line profile was strongly double-peaked, and the predicted CO(2-1) line intensity ($T_A^* = 2$ K) much smaller than that observed ($T_A^* = 8$ K). It was found that a much more satisfactory fit to the CO line data could be obtained by arbitrarily making r_m smaller than r_c . With $r_m = 1.5 \times 10^{16}$ cm and $\dot{M} = 6.5 \times 10^{-7} M_\odot \text{ yr}^{-1}$, we find $T_A^*(1-0) = 0.38$ K for the BTL 7 m telescope and $T_A^*(2-1) = 9.1$ K for the OVRO 10 m telescope, in good agreement with the observations. In both cases, the model line profiles are centrally peaked, in qualitative agreement with the observations. The observations of *o* Cet thus imply that r_m is smaller than r_c for this star (but note that the required value of r_m is much less than that estimated from mapping observations [$\sim 10^{17}$ cm] in Paper I). However, these values of \dot{M} are higher than the values of $\sim 1.2 \times 10^{-7} M_\odot \text{ yr}^{-1}$ deduced from optical line measurements (e.g., Hagen, Stencel and Dickinson 1983) or from the extinction (e.g., Knapp 1985, hereafter Paper IV). The star is known to have a compact companion, and it is possible that the *o* Cet circumstellar shell is a bipolar nebula seen pole-on; this could lead to a centrally peaked line with the larger value of r_m and a smaller value of \dot{M} ($1.2 \times 10^{-7} M_\odot \text{ yr}^{-1}$; cf. also Paper I).

CRL 482.—The present measurements are rather uncertain because of the contamination of the line profile by galactic-plane CO emission. Our distance estimate (1600 pc) is lower than that of RH (2300 pc).

IRC + 50096.—The value of \dot{M} found here ($6.3 \times 10^{-6} M_{\odot} \text{ yr}^{-1}$) is about 3 times smaller than the value derived in Paper I. Most of this difference is due to the higher value of f assumed here. The distance estimate used here (680 pc) is in reasonable agreement with RH's value of 760 pc, and the value of V_o is in good agreement with previous values.

NML Tau.—The present value of \dot{M} , $5.1 \times 10^{-6} M_{\odot} \text{ yr}^{-1}$, is in reasonably good agreement with the value of 4.2×10^{-6} found in Paper I. The value of V_o found here, 22 km s^{-1} , lies in the midrange of previous values in the literature (17–28 km s^{-1}). The distance estimate of RH (520 pc) is about twice that used here.

IRC + 60144.—The present CO data provide the only mass loss estimate available for this star. The value of \dot{M} , $2.3 \times 10^{-5} M_{\odot} \text{ yr}^{-1}$, is in reasonable agreement with the value obtained from the simpler formulation of Paper I, $3.0 \times 10^{-5} M_{\odot} \text{ yr}^{-1}$. However, the position used for these observations (Table 1) was $\sim 25''$ from the accurate position given by Kleinmann and Payne-Gaposchkin (1979), and our value of T_A^* , and hence \dot{M} , may be underestimated by $\sim 20\%$ as a result of this position error.

CRL 618.—Model profiles for this star are given in Figure 17. The predicted value of T_A^* (NRAO) is 0.95 K, higher than the observed value ($T_A^* = 0.60$ K). However, the predicted CO(2–1) temperature (Table 8) is in satisfactory agreement with the observed value in Paper I, as is the predicted CO(1–0) temperature for Onsala ($T_A^* = 2.8$ K; $T_A^* = 2.9$ K), and the derived mass loss rate, $7.7 \times 10^{-5} M_{\odot} \text{ yr}^{-1}$, agrees reasonably well with that suggested by Jura (1983*b*). This present value is about half of that derived in Paper I ($1.6 \times 10^{-4} M_{\odot} \text{ yr}^{-1}$) because of the larger value of f assumed here.

IRC + 60150.—The value of \dot{M} found here, $1.1 \times 10^{-6} M_{\odot} \text{ yr}^{-1}$, is about a third of that found in Paper I. Most of the difference can be attributed to the much smaller value of V_o (12.5 km s^{-1}) found here as compared with the value quoted in Paper I (18 km s^{-1}). The distance estimate of RH, 220 pc, is smaller than the value 360 pc used here.

R Lep.—The uncertain detection reported here provides the only estimate so far of the mass loss rate for this star. The distance used here is 450 pc, but the P - M_v relationship of van den Bergh (1984) suggests a smaller distance, 140 pc.

IRC + 50137.—The value of \dot{M} found here, $6.5 \times 10^{-6} M_{\odot} \text{ yr}^{-1}$, is similar to that found by Bowers, Johnston, and Spencer (1983) and Booth, Diamond, and Norris (1984) from OH measurements ($\dot{M} \sim 10^{-5} M_{\odot} \text{ yr}^{-1}$). It is several times smaller than the value quoted in Paper II, mostly because of the smaller values used here for the distance and outflow velocity. The value of V_o found from the present observations, 14.7 km s^{-1} , may be an underestimate; the OH measurements of Bowers, Johnston, and Spencer (1983) give $V_o = 17.7 \text{ km s}^{-1}$.

R Aur.—Distance estimates from period- M_v relationships give similar values; that used by Bowers and Hagen (1984) gives 366 pc, while that of van den Bergh (1984) gives 380 pc. The value of \dot{M} found here, $5.3 \times 10^{-7} M_{\odot} \text{ yr}^{-1}$, is about a third of the value which would be derived from the equations of Paper I; the difference can be attributed to the inclusion of the effects of stellar IR excitation in the present calculations.

IRC + 70066.—The distance estimate used here, 800 pc, is lower than that of RH ($D = 1220$ pc). The mass loss rate found

here, $1.1 \times 10^{-5} M_{\odot} \text{ yr}^{-1}$, agrees well with that found using the formulae in Paper I, i.e., $\dot{M} = 1.5 \times 10^{-5} M_{\odot} \text{ yr}^{-1}$.

α Ori.—Recent estimates for the mass loss rate for α Ori vary considerably, although they average a few times $10^{-6} M_{\odot} \text{ yr}^{-1}$ if the assumed distance is 200 pc. For example, from observations of light scattered in the K I $\lambda 7699$ resonance line, Mauron *et al.* (1984) conclude that $\dot{M} = 4 \times 10^{-6} M_{\odot} \text{ yr}^{-1}$, and Hagen, Stencel, and Dickinson (1983) find $\dot{M} = 3 \times 10^{-6} M_{\odot} \text{ yr}^{-1}$ from their interpretation of the Sr II absorption line. On the other hand, if the gas-to-dust ratio is normal, then the circumstellar dust abundance gives $\dot{M} = 5.2 \times 10^{-7} M_{\odot} \text{ yr}^{-1}$ (Paper IV), consistent with that suggested by Sanner (1976).

Setting aside the existing information about the size of the CO emission region, we can model the $J = 1 \rightarrow 0$ intensity with $\dot{M} = 1.3 \times 10^{-7} (3 \times 10^{-4}/f) M_{\odot} \text{ yr}^{-1}$ and $r_m = r_c = 1.3 \times 10^{17}$ cm. This mass loss rate appears to be untenably low; moreover, the $J = 2-1$ intensity is poorly fitted (0.2 K predicted vs. 1.1 K observed), and the model profiles are strongly double-peaked, unlike those observed. If we instead adopt the envelope radius observed (Knapp, Phillips, and Huggins 1980), viz., $r_m = 3 \times 10^{16}$ cm, agreement with the CO(1–0) data is obtained with $\dot{M} = 6 \times 10^{-7} M_{\odot} \text{ yr}^{-1} (3 \times 10^{-4}/f)$, and better agreement (0.6 K) is obtained with the CO(2–1) data.

It is difficult to understand why r_m should be small for the α Ori envelope, since circumstellar dust extends to $\sim 2.7 \times 10^{17}$ cm (McMillan and Tapia 1978). The circumstellar molecular envelope may be truncated by UV radiation, e.g., arising from the star's recently discovered hot companion (Goldberg 1984) or if the star is actually in the Orion association at a distance of 400 pc. At this distance we obtain good fits to the data with $\dot{M} = 1.4 \times 10^{-6} (3 \times 10^{-4}/f) M_{\odot} \text{ yr}^{-1}$ and $r_m = 6 \times 10^{16}$ cm. These values will be assumed in subsequent discussion.

CRL 865.—The distance estimate used herein, 1600 pc, agrees reasonably well with that of RH (1300 pc) and the value of the outflow velocity V_o , 15.3 km s^{-1} , is in reasonable agreement with the value measured in Paper I, 14.2 km s^{-1} . However, the CO(1–0) line intensity measured here is only about half of that expected on the basis of the CO(2–1) line intensity (Paper I). The mass loss rate found here, 2.3×10^{-5} , is 7 times lower than that found in Paper I. Part of this discrepancy is due to the larger value of f used in the present calculations, and part to the differences in the observed line intensities.

IRC + 60169.—The measurements reported herein give the only values to date of the distance, mass loss rate, etc., for this star.

OH 231.8+4.2 The model profiles are given in Figure 17. The derived value of \dot{M} , $1.3 \times 10^{-4} M_{\odot} \text{ yr}^{-1}$, is in good agreement with the value of $\dot{M} = 1.3 \times 10^{-4} M_{\odot} \text{ yr}^{-1}$ found from OH measurements (Morris, Bowers, and Turner 1982; Bowers and Morris 1984). However, the value of the outflow velocity V_o found from the CO observations ($68 \pm 12 \text{ km s}^{-1}$) is larger than that (51 km s^{-1}) found from the OH observations, although the central velocities of both lines are similar [$V_c(\text{CO}) = +25$, $V_c(\text{OH}) = +32$], and much larger than the value of 20 km s^{-1} measured at Nobeyama by Zuckerman (1984, private communication). The value of \dot{M} given in Table 6 for this star may thus be too large by about a factor of 10. This large value is, however, supported by the value found from OH observations, quoted above, and the large value of the $400 \mu\text{m}$ flux found by Sopka *et al.* (1984). The distance measurement for this star is based on OH phase-lag observations (Bowers and Morris 1984) and is therefore reasonably

accurate; however, observations of the CO(1–0) line with better sensitivity are necessary to provide more reliable estimates of \dot{M} .

RS Cnc.—The mass loss rate for this star is very poorly known. The distance estimate used in this paper (410 pc) agrees with neither the value given by RH (170 pc) nor that calculated from van den Bergh's $P-M_v$ relationship (880 pc). There are at least two problems with this last distance estimate, however. First, the star is a semiregular variable, so that application of this $P-M_v$ relationship may not be appropriate, and, second, the model atmosphere calculations of Scargle and Strecker (1979) indicate that the extinction (circumstellar plus interstellar) is large ($E_{B-V} = 0.62$ mag).

Apart from distance problems, the value of \dot{M} quoted in Table 7 ($2.9 \times 10^{-7} M_{\odot} \text{ yr}^{-1}$) is a factor of 10 less than that found in Paper I ($3.4 \times 10^{-6} M_{\odot} \text{ yr}^{-1}$). This can be attributed to the effect of taking into account the IR expectation of the CO emission in the present paper, and to the difference in the values of V_0 (measured to be 5.3 km s^{-1} in the present paper, taken from the literature as 11 km s^{-1} in Paper I).

R Leo.—The distance used here, 304 pc, found by Bowers (private communication) using the methods of Bowers and Hagen (1984), is in disagreement with the value of RH (102 pc) and that found from van den Bergh's (1984) $P-M_v$ relationship, 1040 pc. The last value again may be much overestimated—Scargle and Strecker (1979) find $E_{B-V} = 1.2$ mag for this star. Apart from distance errors, the value of \dot{M} found here ($9.2 \times 10^{-8} M_{\odot} \text{ yr}^{-1}$) is a factor of 10 lower than that found in Paper I ($8.5 \times 10^{-7} M_{\odot}$). Again, this can be attributed to the inclusion of IR excitation in the present work and to the lower value of V_0 (4 km s^{-1} versus 7 km s^{-1}). However, the value of V_0 found herein is smaller than that found from the thermal SiO line (Morris *et al.* 1979) and the SiO maser lines (Dickinson *et al.* 1978), and our value of \dot{M} may be too low by about a factor of 2 (apart from distance uncertainties).

IRC + 10216.—The model line profiles are given in Figure 17. The value of \dot{M} ($5.5 \times 10^{-5} M_{\odot} \text{ yr}^{-1}$) is in reasonable agreement with the value of $\sim 6 \times 10^{-5} M_{\odot} \text{ yr}^{-1}$ found by Kwan and Linke (1982) when their results are converted to our assumed distance (290 pc) and CO abundance (8×10^{-4}). The model values of T_A^{\dagger} are in good agreement with the NRAO observations and in reasonable agreement with the OVRO CO(2–1) observations (Table 8). The distance estimate of RH (260 pc) agrees well with that used here. The value of \dot{M} derived here is lower than that in Paper I because of the higher assumed value of f .

CIT 6.—The source is resolved on a scale of $30''$, as observed directly by Nyman, Sahai, and Wannier (1985). The mass loss rate found here, $3.0 \times 10^{-6} M_{\odot} \text{ yr}^{-1}$, is similar to values found by Sahai, Wootten, and Clegg (1984) ($3.2 \times 10^{-6} M_{\odot} \text{ yr}^{-1}$), Henkel *et al.* (1985) ($6 \times 10^{-6} M_{\odot} \text{ yr}^{-1}$), and in Paper I ($3.2 \times 10^{-6} M_{\odot} \text{ yr}^{-1}$). The distance used here, 190 pc, is smaller than that estimated by RH (400 pc).

IRC - 10236.—The value of V_0 found here, 10.9 km s^{-1} , is in reasonable agreement with the value of 10 km s^{-1} quoted in Paper I, although our distance of 950 pc is in disagreement with that of RH (550 pc). The value of \dot{M} , 4.7×10^{-6} , is again about one-third of that found in Paper I, because of the higher value of f used here.

V Hya.—For this star, the distance value assumed here (400 pc) is in good agreement with that of RH (390 pc). The derived value of \dot{M} ($4 \times 10^{-6} M_{\odot} \text{ yr}^{-1}$) is about half the value found in Paper I, owing to the higher value of f assumed here.

Y CVn.—The distance used here, 350 pc, is higher than that of RH (250 pc). Otherwise, the present results give the first available estimate of the mass loss from this star. The distance to the star is likely to be difficult to measure—the extinction toward it is high (Scargle and Strecker 1979 estimate $E_{B-V} = 1.3$ mag).

RU Vir.—The distance for this star is very uncertain; that used in the present work (1470 pc) is about twice the value (700 pc) predicted by van den Bergh's (1984) $P-M_v$ relationship.

RT Vir.—Both the distance and the outflow velocity for this star are very uncertain. The $P-M_v$ relationships give quite different values for the distance: that of Bowers and Hagen (1984) gives 697 pc, while that of van den Bergh (1984) gives 2374 pc. The value of V_0 found in this paper is 11.3 km s^{-1} , while that found by Morris *et al.* (1979) is 7 km s^{-1} . The value of \dot{M} given in Table 7 for this star is thus extremely uncertain.

RX Boo.—The distance used in this paper, 225 pc, is in good agreement with that of RH ($D = 200$ pc). The mass loss rate derived here, $3.8 \times 10^{-7} M_{\odot} \text{ yr}^{-1}$, is 5 times smaller than the value found in Paper I. Some of this difference can be attributed to the influence of the inclusion of IR excitation, but, as is illustrated in Table 8, there is a discrepancy of about a factor of 3 between the CO(2–1) observations of Paper I and the present CO(1–0) observations. The outflow velocity found in the present paper, 11.5 km s^{-1} , is in good agreement with values found from SiO maser and thermal emission (Dickinson *et al.* 1978; Morris *et al.* 1979), but higher than the value of 8 km s^{-1} found in Paper I.

IRC + 20326.—The distance value used here, 1200 pc, is in disagreement with that of RH (690 pc). The value of V_0 agrees well with that given by previous CO observations (cf. Paper I). The value of \dot{M} found here is about 4 times less than that given in Paper I; much of the discrepancy can be attributed to the higher value of f assumed here.

T Dra.—The distance estimates for this star are rather discrepant; the value used here is 525 pc, van den Bergh's (1984) period-luminosity relationship gives 318 pc, and RH give 750 pc.

CRL 2155.—The value of V_0 found here, 15 km s^{-1} , is lower than that quoted in Paper I (20 km s^{-1}), and the value of \dot{M} is 4 times lower. This can be attributed to the higher value of f assumed here and to the discrepancies in the values of V_0 .

CRL 2199.—The value of V_0 found here, 8 km s^{-1} , is half the value quoted in Paper I. This discrepancy, and the higher value of f assumed here, accounts for the factor of 10 difference between the values found in Paper I and those in the present work.

IRC + 10365.—The value of V_0 found here, 16.7 km s^{-1} , is in reasonable agreement with the maser measurements of 15 km s^{-1} (Dickinson *et al.* 1978) but much lower than the value of 22 km s^{-1} inferred from Zuckerman's (1981) value of ΔV .

IRC + 20370.—The distance estimate used here, 790 pc, is in reasonable agreement with RH's value of 830 pc. The value of V_0 , 15 km s^{-1} , is, however, twice that (8 km s^{-1}) used in Paper I.

W Aql.—The value of V_0 found here, 20 km s^{-1} , is larger than that found for the SiO thermal line (Morris *et al.* 1979) but agrees with that found from previous CO observations (see Paper I). The distance estimate used here (470 pc) agrees very well with that (440 pc) predicted by van den Bergh's (1984) relationship. The value of \dot{M} found here is about half that found in Paper I, and the difference can be attributed to the higher value of f used here.

Vy 2-2.—If it is assumed that this object has a luminosity of $10^4 L_{\odot}$, we find a distance of 9 kpc. This is unlikely for several reasons; the object is visible, and the expected galactic extinction for a distance of 9 kpc is large. Second, the distance of the object from the galactic plane would be ~ 400 pc. We have instead assumed a distance of 1 kpc, which brings mass loss rates derived from the CO and radio continuum observations into agreement.

Vy 2-2 is a radio continuum source and an OH maser, and therefore is likely to be a proto-planetary nebula (Davis, Seaquist, and Purton 1979; Seaquist and Davis 1983). Only one OH component is present, at -62 km s $^{-1}$, and its profile shape suggests that it is the blueshifted (near side) component. Seaquist and Davis (1983) suggest that the reshifted OH component is absorbed by the H II region, which is optically thick at 1.7 GHz. Our tentative detection of CO emission at -44 km s $^{-1}$ supports these conclusions.

The radius of the ionized region is 8×10^{15} cm at 1 kpc (Seaquist and Davis 1983). We calculated our model CO profiles using both this value and 10^{15} cm for the inner radius of the circumstellar shell, but found that it does not make a significant difference to the model line intensities. A comparison of the CO and OH velocities suggests $V_0 = 18$ for the circumstellar material around this object. With our value of \dot{M} ($2.4 \times 10^{-6} M_{\odot} \text{ yr}^{-1}$), we expect a mass of ionized hydrogen of about $9 \times 10^{-5} (D/1 \text{ kpc})^3 M_{\odot}$, in reasonable agreement with the observations of Seaquist and Davis (1983), which give $M(\text{H}^+) \sim 7 \times 10^{-5} (D/1 \text{ kpc})^{2.5} M_{\odot}$.

IRC +10420.—The distance to this object, based on OH observations and galactic kinematics, is probably reasonably well determined. The calculated line profiles are given in Figure 17. Our derived value of \dot{M} , $3.0 \times 10^{-4} M_{\odot} \text{ yr}^{-1}$, is in good agreement with the value derived from OH maser observations (Bowers, Johnston, and Spencer 1983). The CO profile marginally suggests a larger value of the outflow velocity (52 ± 20 km s $^{-1}$) than do the OH (33 km s $^{-1}$) or SiO (34 km s $^{-1}$) observations (Bowers, Johnston, and Spencer 1983; Olofsson *et al.* 1982), although the values of the central velocity are similar for all three lines.

χ Cyg.—The first attempt to fit the emission from this star, assuming a distance of 97 pc (cf. Paper I), failed; the calculated line was strongly double-peaked, and the source was highly resolved, neither of which properties agrees with the observations (Fig. 24, Table 5). A reasonable fit with $D = 390$ pc (see Morris 1980) was obtained. We note, however, that all of the derived distance values (RH; references given in Paper I) are less than 100 pc. The present value of \dot{M} for this star is thus extremely uncertain.

IRC -10529.—The distance estimate used here for this star (620 pc) is in conflict with the value of RH (410 pc). The value of V_0 , 16 km s $^{-1}$, is in good agreement with the value of 17.5 km s $^{-1}$ deduced from Zuckerman's (1981) estimate of ΔV .

V Cyg.—The distance estimate used here, 510 pc, is in reasonable agreement with that of RH (580 pc), and the value of V_0 (13 km s $^{-1}$) agrees well with the value of 14 km s $^{-1}$ found from previous CO observations. The mass loss rate given in Table 7 is about 5 times lower than that of Paper I; the difference is due to the higher value of f used here and to the inclusion of IR excitation.

CRL 2688.—The calculated line profiles are given in Figure 17. The model gives a value of T_A^* for NRAO of 2.4 K, while $T_A^* = 1.7$ K. For Onsala, $T_A^* = 5.5$ K, while $T_A^* = 4.1$ K. For OVRO, $T_A^*(2-1) = 4.4$ K, while $T_A^* = 1.9$ K. These results

suggest that the object is resolved, and may therefore be closer than the assumed distance of 1 kpc. The value of V_0 , 19.7 km s $^{-1}$, is in good agreement with that found in Paper I, and the derived mass loss rates are in good agreement.

IRC +00499.—The only information available for the mass loss rate for this object is given in the present paper.

NGC 7027.—A first model for this object used a value of 10^{15} cm for the inner radius of the circumstellar material; the resulting value of \dot{M} was $9.0 \times 10^{-5} M_{\odot} \text{ yr}^{-1}$. However, the central regions of the circumstellar cloud are ionized, and the H II region radius is $5''$ (e.g., Paper II), or 7.5×10^{16} cm at a distance of 1 kpc. Using this value for the inner radius of the molecular envelope in the models, it was necessary to raise \dot{M} to $1.1 \times 10^{-4} M_{\odot}$ to obtain agreement with the BTL CO(1-0) observation. This value is given in Table 6.

NGC 7027 emits strongly in the CO lines, but emission in other molecular lines, e.g., ^{13}CO (Knapp and Chang 1985), HCN, and CS (Bally 1984), is weak. This is probably because the CO(1-0) emission from molecular envelopes is predominantly from the gas at large radii, while the emission from other, radiatively excited species is from the inner regions of the envelope, which are ionized in the case of NGC 7027 (while ^{13}CO is coextensive with CO, it is largely radiatively excited).

The value of V_0 found here, 18 km s $^{-1}$, is smaller than the value of 22 km s $^{-1}$ quoted in Paper I. The value of \dot{M} is about a third of that found in Paper I, and the difference can be attributed to the higher value of f assumed here.

IRC +40483.—The parameters given for this star in the present paper provide the first estimates of \dot{M} for this object.

IRC +40485.—The distance used here, 780 pc, agrees reasonably well with that of RH (900 pc), and the outflow velocity, 14.9 km s $^{-1}$, is in reasonable agreement with the values in Paper I. The value of \dot{M} is a factor of 6 lower than that given in Paper I, where abundance and radiative excitation effects were not taken into account.

CRL 3068.—The distance used here, 570 pc, is discrepant with RH's value of 1190 pc, while the values of V_0 here and in Paper I agree well. After adjusting for the different distance values used here and in Paper I, the value of \dot{M} found here for this carbon star is several times lower than that found in Paper I.

CRL 3099.—The distance used here, 500 pc, is very discrepant with RH's value of 2100 pc, and the mass loss rate for this star is correspondingly exceedingly uncertain.

IRC +40540.—The distance estimates given here (960 pc) and by RH (940 pc) are in good agreement.

R Cas.—The value of V_0 measured here (12.3 km s $^{-1}$) is in good agreement with previous CO observations (e.g., Paper I) but is higher than that found from SiO data (9 km s $^{-1}$; Morris *et al.* 1979). The values of \dot{M} for this Mira variable found here and in Paper I are in good agreement. Our distance (216 pc) is, however, discrepant with that of RH (122 pc).

b) Mass Loss Statistics

The results obtained for the mass loss rates (corrected for helium content) from the 50 evolved stars studied in this paper are summarized in Figures 22 and 23. Figure 22 shows a histogram of the number of stars per pc 3 versus \dot{M} , Figure 23 shows the mass loss rate per pc 3 versus \dot{M} . In both cases, the stars are divided into those with $[\text{O}] > [\text{C}]$ and those with $[\text{O}] \leq [\text{C}]$.

The space density for stars of a given \dot{M} was calculated by determining a volume corresponding to each star, not from the assumed distance D (Table 4), but from the maximum distance

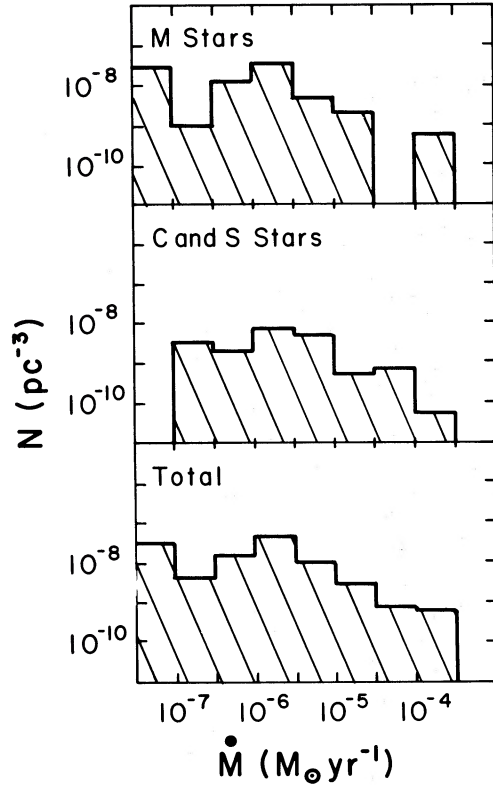


FIG. 22.—Histogram of calculated mass loss rates for evolved stars. The abscissa is $\log \dot{M}$ and the ordinate $\log (N \text{ pc}^{-3})$. The upper panel is for the Mira stars, and the lower panel for carbon and S stars.

D_m at which the star could have been detected in the CO(1–0) line in the present observations. The volumes were then calculated from

$$V = \pi D_m^2 (2.35h), \quad D_m > 1.2h$$

$$= \frac{4\pi}{3} D_m^3, \quad D_m < 1.2h, \quad (9)$$

where h is the Gaussian scale height of the type of star observed [i.e., defined here by $N(z) \sim \exp(-z^2/2h^2)$]. Knapp (1983) showed that h is a function of the outflow velocity V_o , being smallest for the group of stars with the largest values of V_o . The value of h for each star was found from the tabulations by Knapp (1983).

The values of D_m were found from the quantities in Tables 1 and 4 from

$$\frac{D_m}{D} = \left(\frac{2T_A^*}{3T_{\text{rms}}^*} \right)^{1/2} \quad (10)$$

Here, T_A^* is the peak CO line temperature observed for each star, and T_{rms}^* is the noise in the 250 kHz filter bank. It is assumed that a star could be detected if T_A^* is 3 times the noise in the 1 MHz filter banks ($= T_{\text{rms}}^*/2$). As can be seen from Table 1, an observation was carried out to a sensitivity of $T_{\text{rms}}^* = 0.03$ K or until the star was reasonably well detected. Thus a value of 0.03 K was used for T_{rms}^* in equation (10) for all the observations, except those few at low declinations (e.g., R Scl), where increased atmospheric noise renders the observations much less sensitive.

Once the volumes were determined, the reciprocal volumes were then added in each interval of \dot{M} in order to derive the

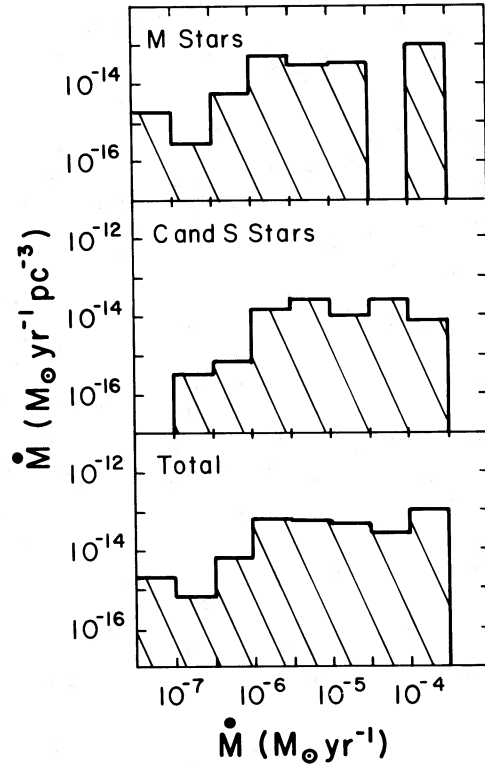


FIG. 23.—Dependence of mass loss rate per unit volume (in $M_\odot \text{ yr}^{-1} \text{ pc}^{-3}$) on mass loss rate \dot{M} . The upper panel is for oxygen stars and the lower panel for carbon and S stars.

density. It must be emphasized at this point that the histogram presented in Figure 22 is not a true “luminosity function” of \dot{M} ; first, the effect of the upper limits (Table 1) has not yet been taken into account. This is deferred to future work, where the data in the present paper will be analyzed. It is unlikely that inclusion of the upper limits will make a large qualitative difference to the comparison between O and C stars in Figure 23, however, since the percentage of detections for the oxygen- and carbon-rich stars is about the same. Second, the influence of selection effects (directly or indirectly, the stars in Table 1 are selected on the basis of their flux at a few microns) has not been investigated, and the CO observations are not sensitive to stars with $\dot{M} \lesssim 3 \times 10^{-8} M_\odot \text{ yr}^{-1}$.

The cutoff at high values of \dot{M} shown in Figure 22 is probably real; here, stars are losing mass at such a rate that they cannot last for long. At the low end ($\dot{M} < 3 \times 10^{-8} M_\odot \text{ yr}^{-1}$) the cutoff is probably due to sensitivity, to selection effects, and to the possibility that at low values of \dot{M} some of the stars may be hotter and their circumstellar material atomic. Within the observed range of \dot{M} , the distributions for the C and O stars are quite similar, although there is a very weak suggestion from Figure 22 (and Fig. 15) that at low values of \dot{M} ($\lesssim 10^{-7} M_\odot \text{ yr}^{-1}$) the oxygen stars dominate.

The distribution of \dot{M} per unit volume (Fig. 23) can now be integrated to estimate the total rate of mass return to the interstellar medium in the Galaxy. The data analyzed herein are representative of the solar neighborhood; let us assume that the evolved stars are part of the disk population, so that their galactic distribution may be described by

$$\Sigma(R) = \Sigma_0 \exp(1 - R/R_0)/\lambda \text{ pc}^{-2} \quad (11)$$

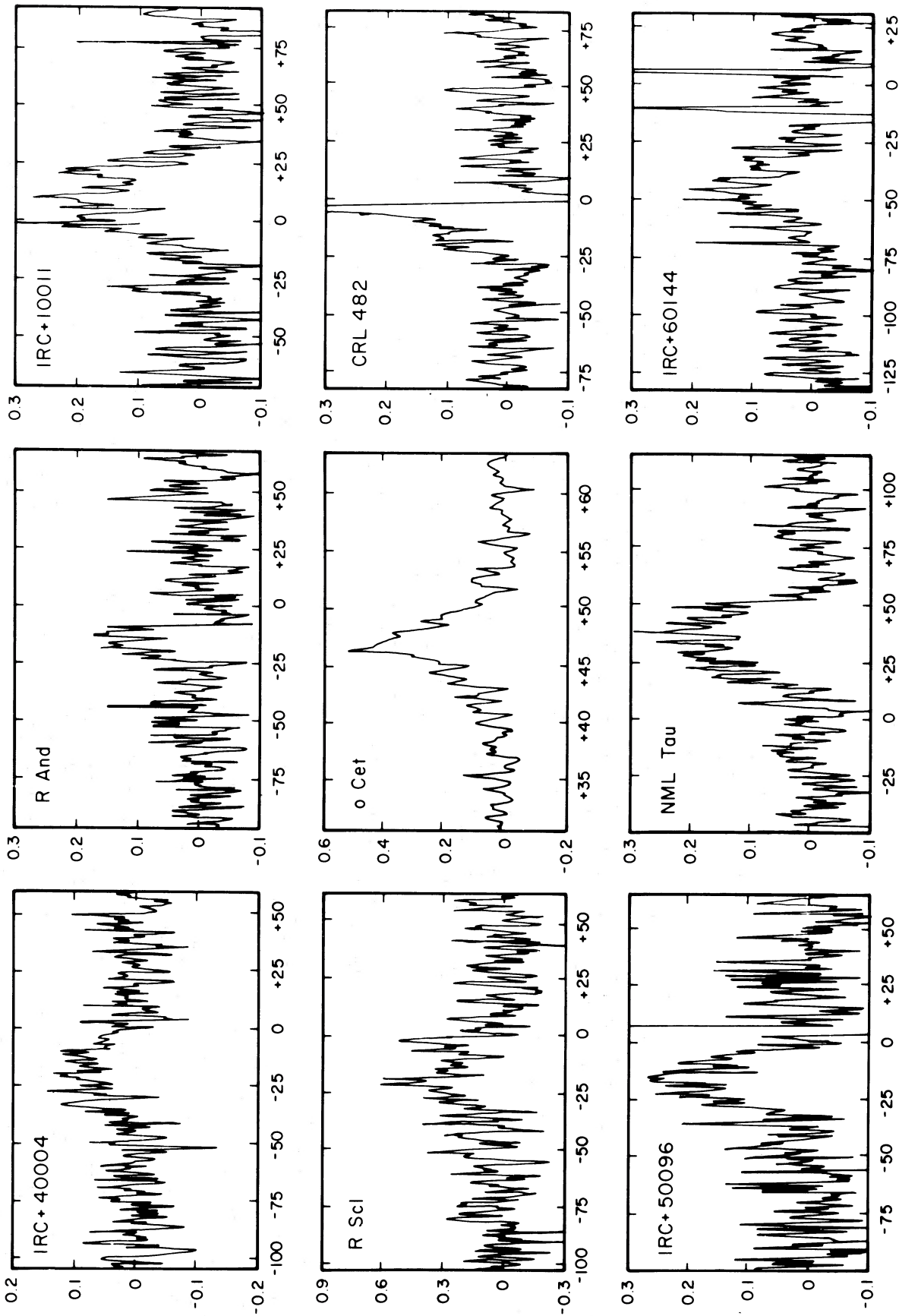


FIG. 24.—CO(1-0) line profiles observed with the Bell Laboratories telescope for 50 evolved stars. The ordinate is $T_{*}(1-0)$ in K; the abscissa is velocity relative to the LSR in km s^{-1} .

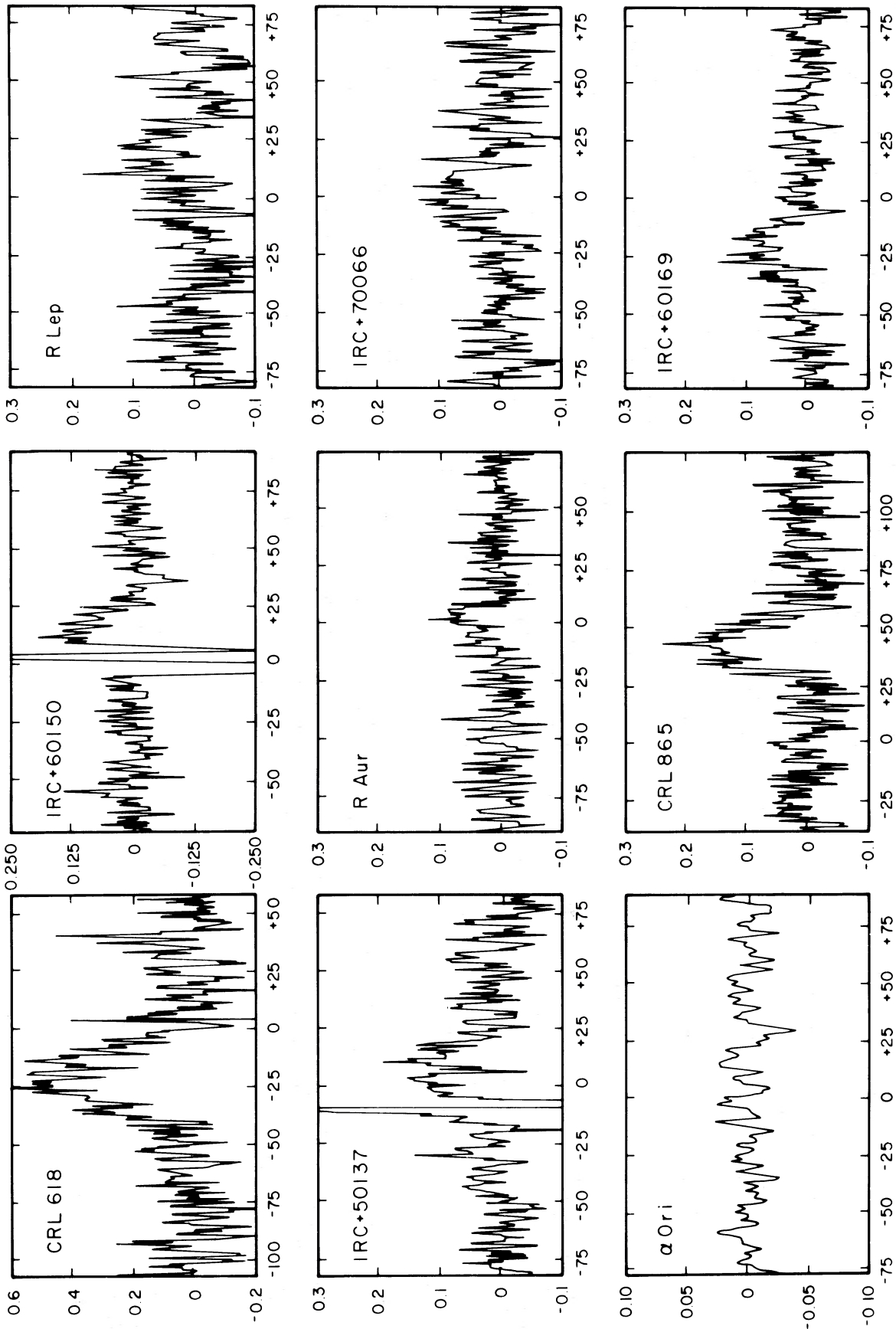


FIG. 24.—Continued

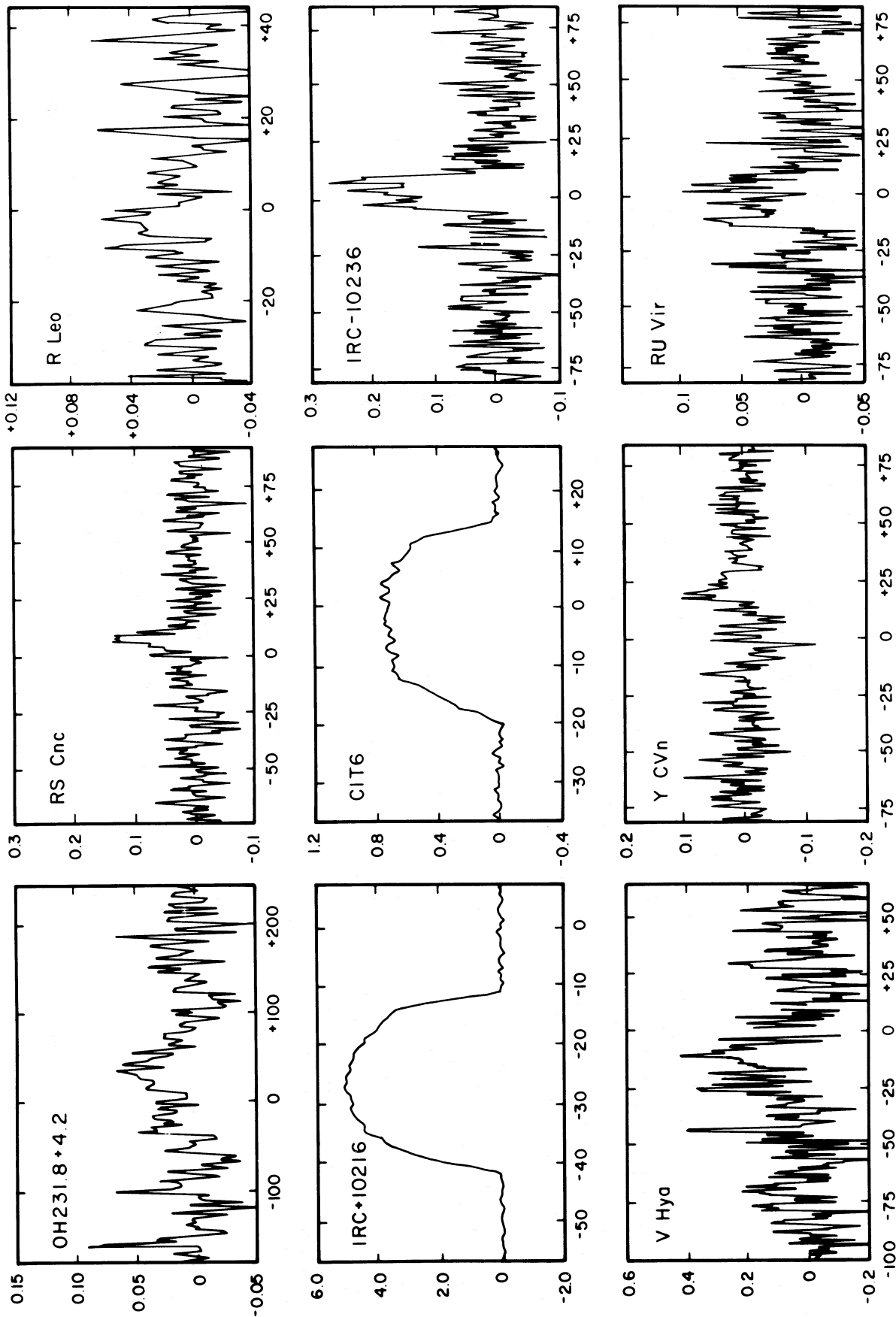


FIG. 24.—Continued

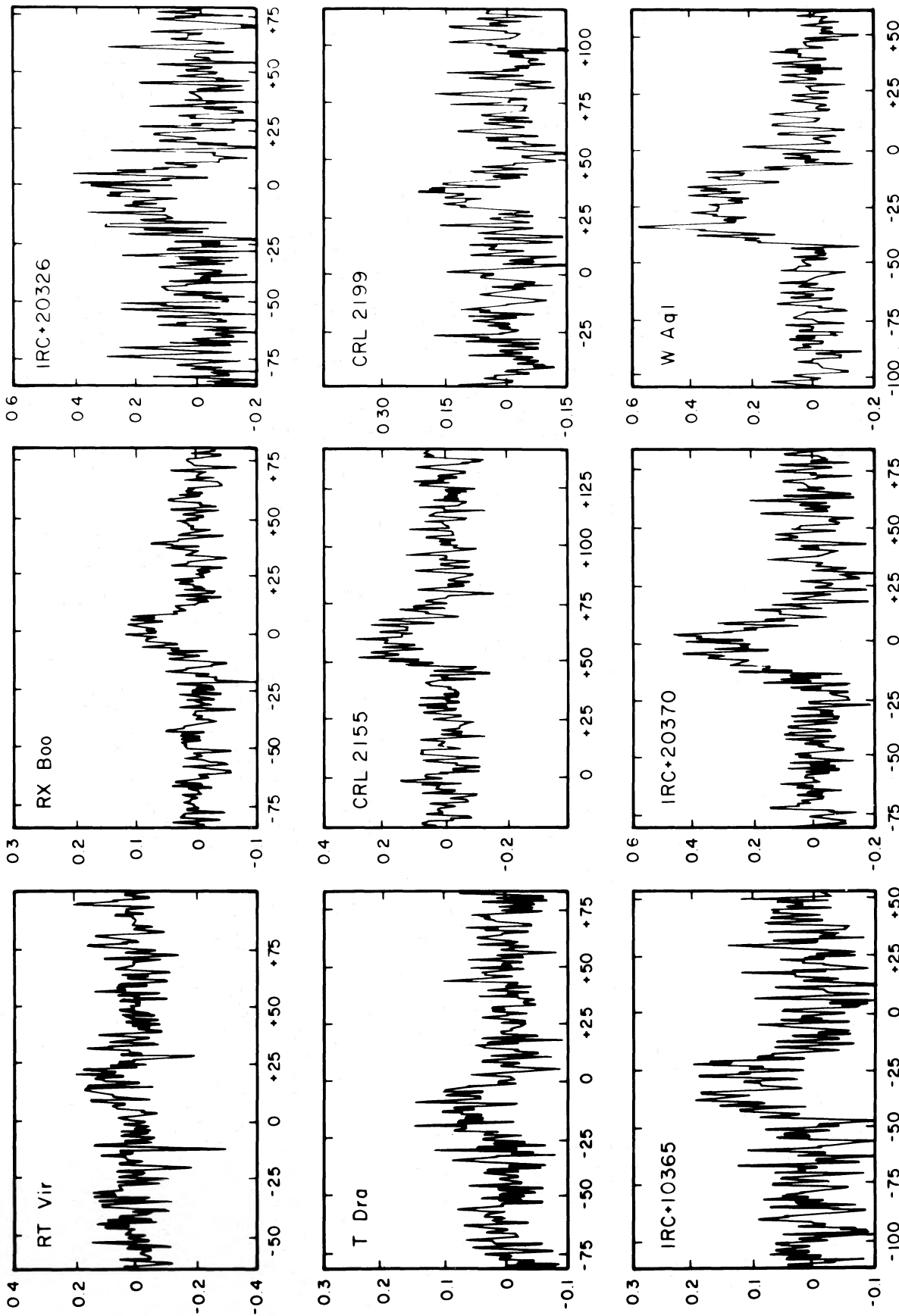


FIG. 24.—Continued

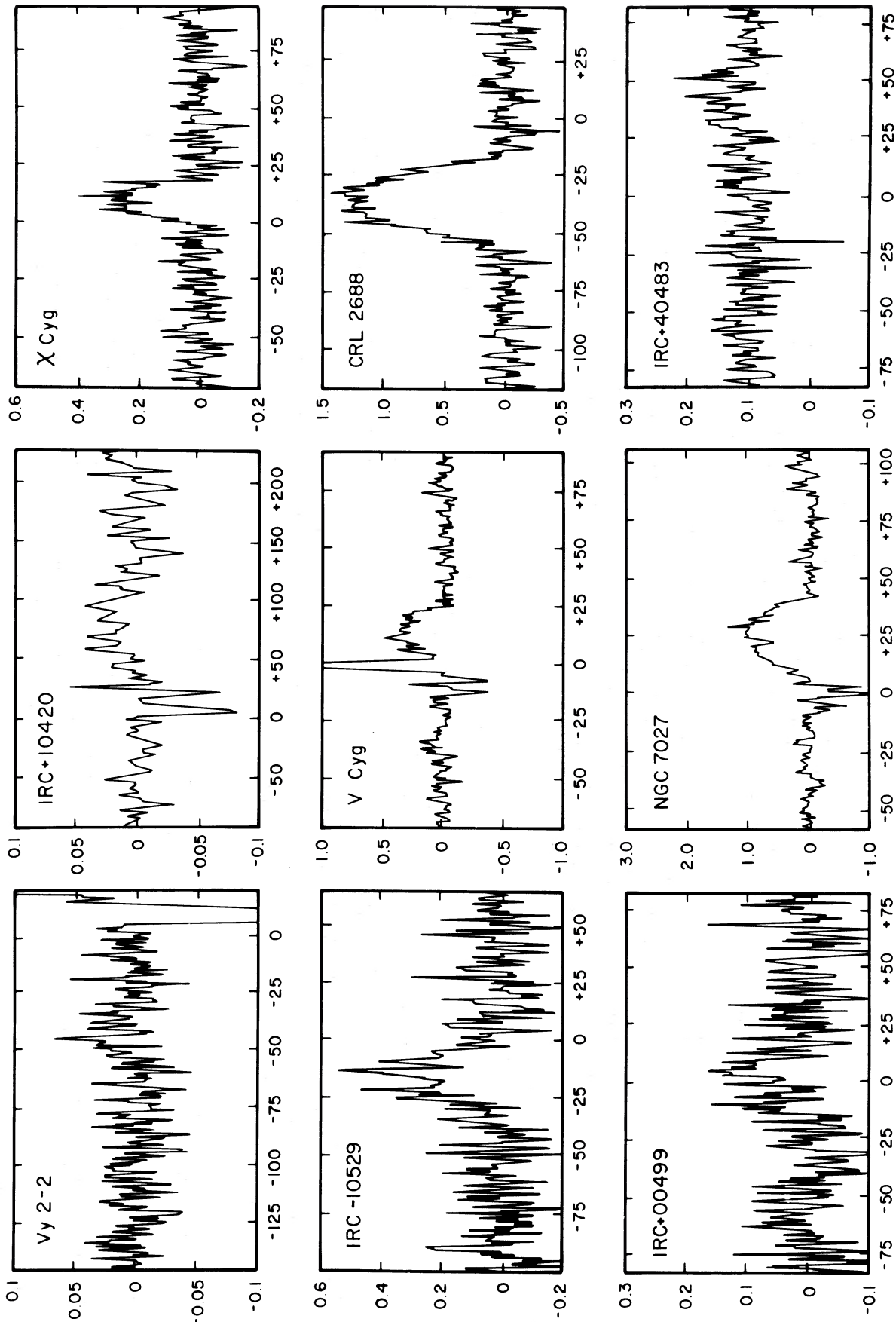


FIG. 24.—Continued

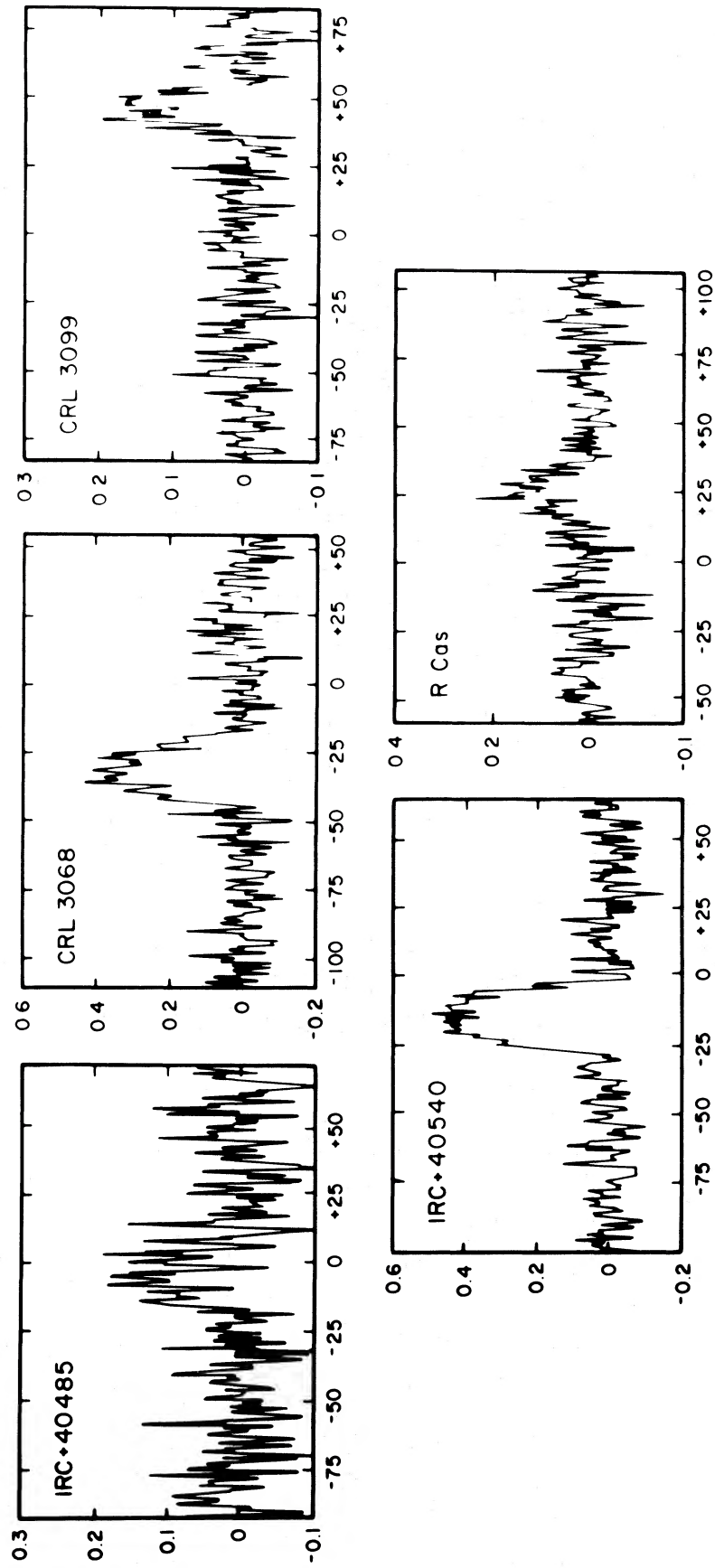


FIG. 24.—Continued

(Knapp, Tremaine, and Gunn 1978), where R_0 is the distance between the Sun and the galactic center, λ is the disk scale length in units of R_0 , and Σ_0 is the surface density of mass-losing stars in the solar neighborhood. Then the total mass loss rate in the Galaxy can be found from

$$\dot{M}_T = \int_0^\infty 2\pi R dR \Sigma(R) \langle \dot{M} \rangle \quad (12)$$

(the fact that the disk does not extend to $R = 0$ is only a small correction), or

$$\dot{M}_T = 2\pi \Sigma_0 R_0^2 \lambda^2 \exp(1/\lambda) \langle \dot{M} \rangle, \quad (13)$$

where $\langle \dot{M} \rangle$ is the mean mass loss rate per mass-losing star, and the correction factor $\lambda^2 \exp(1/\lambda)$ has the value 1.95 for $\lambda = 0.4$. If the scale height is assumed constant at 200 pc (the mean scale height for our group of stars), \dot{M}_T can be found from the values of \dot{M} per unit volume shown in Figure 23.

We can estimate Σ_0 by adding \dot{M} for all the stars within 1 kpc of the Sun, and multiplying by 2 to account for incompleteness due to lack of southern hemisphere observations (although objects as far south as -30° have been observed, the sensitivity at low declinations is very poor because of atmospheric extinction). This gives $\langle \dot{M} \rangle \Sigma_0 = 2 \times 10^{-10} M_\odot \text{ yr}^{-1} \text{ pc}^{-2}$, or, using equation (13), $\dot{M}_T = 0.17 M_\odot \text{ yr}^{-1}$ ($R_0 = 8.5$ kpc). We can also integrate the distributions in Figure 23, again multiply by 2, and find $\dot{M}_T = 0.28 M_\odot \text{ yr}^{-1}$. The difference suggests that a substantial contribution to \dot{M}_T comes from the very few stars losing mass at $\gtrsim 10^{-4} M_\odot \text{ yr}^{-1}$; these stars, being few and far between, are found at great distances.

We note that these values of the total galactic mass loss rate are not much affected by distance errors, since \dot{M} scales as D^2 , while the surface density of stars scales as D^{-2} .

V. SUMMARY AND CONCLUSIONS

The results of this paper can be summarized as follows:

1. A total of 105 evolved stars was surveyed in the CO(1–0) line using the Bell Laboratories 7 m telescope. CO emission from circumstellar shells formed by cool winds was detected for 50 stars (including seven tentative detections), with 20 stars detected for the first time in the CO(1–0) line. The line profiles give values for the stellar systemic velocity and the terminal wind outflow velocity, as well as some information on the opacity of the envelope and on the degree to which it is resolved by the antenna. Monitoring of the CO line profile for CIT 6 failed to find significant evidence for variability.

2. A series of models for the CO emission from the envelopes, incorporating the effects of collisions, IR excitation, and radiative trapping, was calculated. These models fall into two classes: those for which the envelope is opaque to both the

$v = 0 \rightarrow 1$ line (radially) at $4.6 \mu\text{m}$ and the $J = 1-0$ line (tangentially) at 2.6 mm , with the result that IR excitation is unimportant; and those for which the envelopes are more or less transparent in the IR lines and the primary excitation is from stellar or near-circumstellar IR emission.

3. The models were fitted to the observed data. It was found that about half of the objects fall into each category. The fitting necessarily involves compromises, since many of the necessary quantities (e.g., distance, outer envelope radius) are known poorly or not at all.

4. The model fitting also took rough account of the effects of CO dissociation by interstellar UV. It was found that the critical dissociation radius is large enough to be unimportant ($\gtrsim 10^{18} \text{ cm}$) for the line profiles from "optically thick" envelopes.

5. Most of the optically thick envelopes were found to have their emissivity limited by the low particle density (hence low collision rate) at large radii, while the optically thin envelopes are likely to be limited in radius by dissociation by interstellar UV.

6. The models allow the construction of an approximate formula giving values of \dot{M} for the stars from the CO observations. The data presented herein and by others weakly suggest that the values of f are 2–3 times higher for the carbon stars than for the oxygen stars, although more data are needed to demonstrate this conclusively.

7. The derived values of \dot{M} cover the range $\sim 3 \times 10^{-8}$ to $\sim 2 \times 10^{-4} M_\odot \text{ yr}^{-1}$. The range is similar for oxygen-rich and C stars; however, most of the stars losing mass at a rate \lesssim a few $\times 10^{-7} M_\odot \text{ yr}^{-1}$ are oxygen-rich stars.

8. The total amount of mass returned to the interstellar medium for the Galaxy is estimated to be $\sim 0.3 M_\odot \text{ yr}^{-1}$ from these observations; this is probably a lower limit because of selection effects.

The line profiles for the 50 stars from which CO(1–0) emission was observed are shown in Figure 24.

We thank Kar Man Chang for much valuable help with the computing. We are indebted to J. Bally, R. A. Linke, A. A. Stark, and R. W. Wilson for the use of the astronomical observing facilities at Bell Laboratories; to R. W. Wilson for help with the computing and data reduction; and to R. E. Miller for fabricating the SIS junctions. We thank S. Green for providing up-to-date revisions of the CO cross sections. We thank J. E. Gunn and M. Jura for many valuable suggestions, L. Å. Nyman and P. G. Wannier for communicating data before publication, and B. Zuckerman for helpful comments on the manuscript. This research was partly supported by NSF grants AST80-09252 and AST82-13293 to Princeton University.

REFERENCES

- Alksnis, A., and Khovov, G. V. 1975, *Soviet AJ (Letters)*, **1**, 23.
 Allen, C. W. 1973, *Astrophysical Quantities* (London: Athlone).
 Altamore, A., Smriglia, F., Bussoletti, E., Corsi, C. E., and Rossi, L. 1980, *Ap. Space Sci.*, **72**, 159.
 Bally, J. 1984, private communication.
 Bevington, P. R. 1969, *Data Reduction and Error Analysis for the Physical Sciences* (New York: McGraw-Hill).
 Booth, R. S., Diamond, P. J., and Norris, R. P. 1984, in *IAU Symposium 110, VLBI and Compact Radio Sources*, ed. R. Fanti, K. I. Kellermann, and G. Setti (Dordrecht: Reidel), p. 313.
 Bowers, P. F., and Hagen, W. 1984, *Ap. J.*, **285**, 637.
 Bowers, P. F., Johnston, K. J., and Spencer, J. H. 1981, *Nature*, **291**, 382.
 ———. 1983, *Ap. J.*, **274**, 733.
 Bowers, P. F., and Morris, M. 1984, *Ap. J.*, **276**, 646.
 Buhl, D., Snyder, L. E., Lovas, F. J., and Johnson, D. R. 1975, *Ap. J. (Letters)*, **201**, L29.
 Castor, J. I. 1970, *M.N.R.A.S.*, **149**, 111.
 Celis, L. 1981, *Astr. Ap.*, **99**, 58.
 ———. 1984, *A.J.*, **89**, 1343.
 Chapman, S., and Green, S. 1977, *J. Chem. Phys.*, **67**, 2317.
 Cohen, M. 1979, *M.N.R.A.S.*, **186**, 837.
 ———. 1980, *Ap. J. (Letters)*, **238**, L81.
 Cummins, S. E., Morris, M., and Thaddeus, P. 1980, *Ap. J.*, **235**, 886.
 Davis, L. E., Seaquist, E. R., and Purton, C. R. 1979, *Ap. J.*, **230**, 434.
 Dickinson, D. F., Snyder, L. E., Brown, L. W., and Buhl, D. 1978, *A.J.*, **83**, 36.
 Forrest, W. J., Gillett, F. G., and Stein, W. A. 1975, *Ap. J.*, **195**, 423.
 Frogel, J. A., Dickinson, D. F., and Hyland, A. R. 1975, *Ap. J.*, **201**, 392.
 Fujita, Y., and Tsuji, T. 1977, *Proc. Astr. Soc. Japan*, **29**, 711.
 Gezari, D. Y., Schmitz, M., and Mead, J. M. 1982, NASA Tech. Mem. 83819.
 Gillett, F. C., Merrill, K. M., and Stein, W. A. 1971, *Ap. J.*, **164**, 83.
 Goebel, J., et al. 1980, *Ap. J.*, **235**, 104.
 Goldberg, L. 1984, private communication.

- Hackwell, J. A. 1972, *Astr. Ap.*, **21**, 239.
 Hagen, W., Stencel, R. F., and Dickinson, D. F. 1983, *Ap. J.*, **274**, 386.
 Henkel, C., Matthews, H. E., Morris, M., Terebey, S., and Fich M. 1985, *Ap. J.*, submitted.
 Herbig, G. H. and Zappala, R. R. 1970, *Ap. J. (Letters)*, **162**, L15.
 Hyland, A. R., Becklin, E. E., Frogel, J. A., and Neugebauer, G. 1972, *Astr. Ap.*, **16**, 204.
 Jura, M. 1983a, *Ap. J.*, **267**, 647.
 ———. 1984, private communication.
 ———. 1983b, *Ap. J.*, **275**, 683.
 Kleinmann, S. G., and Payne-Gaposchkin, C. 1979, *Earth Extraterr. Sci.*, **3**, 161.
 Knapp, G. R., 1983, in *IAU Colloquium 76, The Nearby Stars and the Stellar Luminosity Function*, ed. A. G. Davis Philip and Arthur R. Upgren (Schenectady: Davis), p. 113.
 ———. 1985, *Ap. J.*, in press (Paper IV).
 Knapp, G. R., and Chang, K.-M. 1985, *Ap. J.*, in press.
 Knapp, G. R., Kuiper, T. B. H., and Zuckerman, B. 1979, *Ap. J.*, **233**, 140.
 Knapp, G. R., Phillips, T. G., and Huggins, P. J. 1980, *Ap. J. (Letters)*, **242**, L25.
 Knapp, G. R., Phillips, T. G., Leighton, R. B., Lo, K.-Y., P. G., Wootten, H. A., and Huggins, P. J. 1982, *Ap. J.*, **252**, 616 (Paper I).
 Knapp, G. R., Tremaine, S. D., and Gunn, J. E. 1978, *A.J.*, **83**, 1585.
 Kuiper, T. B. H., Knapp, G. R., Knapp, S. L., and Brown, R. L. 1976, *Ap. J.*, **204**, 408.
 Kwan, J., and Hill, F. 1977, *Ap. J.*, **215**, 781.
 Kwan, J., and Linke, R. A. 1982, *Ap. J.*, **154**, 587.
 Lada, C. J., and Reid, M. J. 1978, *Ap. J.*, **219**, 95.
 Lambert, D. L., and Vanden Bout, P. A. 1978, *Ap. J.*, **221**, 854.
 Linke, R. A., Schneider, M. V., and Cho, A. Y. 1978, *IEEE Trans.*, **MTT-26**, 935.
 Lo, K.-Y., and Bechis, K. P. 1976, *Ap. J.*, (*Letters*), **205**, L21.
 ———. 1977, *Ap. J. (Letters)*, **218**, L27.
 Mauron, N., Fort, B., Querci, F., Dreux, M., Fauconnier, T., and Lamy, P. 1984, *Astr. Ap.*, **130**, 341.
 McKee, C. F., Storey, J. W. V., Watson, D. M., and Green, S. 1982, *Ap. J.*, **259**, 647.
 McMillan, R. S., and Tapia, S. 1978, *Ap. J. (Letters)*, **266**, L87.
 Merrill, K. M., and Stein, W. A. 1976, *Pub. A.S.P.*, **88**, 294.
 Morris, M. 1975, *Ap. J.*, **197**, 603.
 ———. 1980, *Ap. J.*, **236**, 823.
 Morris, M., and Alcock, C. 1977, *Ap. J.*, **218**, 687.
 Morris, M., Bowers, P. F., and Turner, B. E. 1982, *Ap. J.*, **259**, 625.
 Morris, M., and Jura, M. 1983, *Ap. J.*, **264**, 546.
 Morris, M., Lucas, R., and Omont, A. 1985, in preparation.
 Morris, M., Redman, R. O., Reid, M. J., and Dickinson, D. F. 1979, *Ap. J.*, **229**, 257.
 Mufson, S. L., and Liszt, H. S. 1975, *Ap. J.*, **202**, 183.
 Mufson, S. L., Lyon, J., and Marionni, P. A. 1975, *Ap. J. (Letters)*, **201**, L85.
 Ney, E. P., Merrill, K. M., Becklin, E. E., Neugebauer, G., and Wynn-Williams, G. 1975, *Ap. J. (Letters)*, **198**, L129.
 Nyman, L. A., Sahai, R., and Wannier, P. G. 1985, in preparation.
 Olofsson, H., Johansson, L. E. B., Hjalmarsen, A., and Nguyen-Q-R. 1982, *Astr. Ap.*, **107**, 128.
 Phillips, T. G., Jefferts, K. B., and Wannier, P. G. 1974, *Ap. J. (Letters)*, **192**, L53.
 Phillips, T. G., Woody, D. P., Dolan, G. J., Miller, R. E., and Linke, R. A. 1981, *IEEE Trans.*, **MAG-17**, 684.
 Pottasch, S. R., Goss, W. M., Arnal, M., and Gathier, R. 1982, *Astr. Ap.*, **106**, 229.
 Price, S. D., and Walker, R. G. 1976, Air Force Geophysical Laboratory, Tech. Rept. 76-0208.
 Rodriguez Kuiper, E. N., Kuiper, T. B. H., Zuckerman, B., and Kakar, R. K. 1977, *Ap. J.*, **214**, 394.
 Rowan-Robinson, M., and Harris, S. 1982, *M.N.R.A.S.*, **200**, 197.
 ———. 1983a, *M.N.R.A.S.*, **202**, 767.
 ———. 1983b, *M.N.R.A.S.*, **202**, 797 (RH).
 Sahai, R., Wootten, H. A., and Clegg, R. E. S. 1984, *Ap. J.*, **284**, 144.
 Sanner, F. 1976, *Ap. J. Suppl.*, **32**, 115.
 Scargle, J. D., and Strecker, D. W. 1979, *Ap. J.*, **228**, 838.
 Seaquist, E. R., and Davis, L. E. 1983, *Ap. J.*, **274**, 659.
 Smak, J. 1966, *Ann. Rev. Astr. Ap.*, **4**, 19.
 Solomon, P. M., Jefferts, K. B., Penzias, A. A., and Wilson, R. W. 1971, *Ap. J. (Letters)*, **163**, L53.
 Sopka, R. J., Hildebrand, R., Jaffe, D. T., Gatley, I., Roellig, T., Werner, M. W., Jura, M., and Zuckerman, B. 1985, preprint.
 Spiegel, D. N., Giuliani, J. L., and Knapp, G. R. 1983, *Ap. J.*, **275**, 330 (Paper II).
 Strecker, D. W., and Ney, E. P. 1974, *A.J.*, **79**, 1410.
 Thaddeus, P., Cummins, S. E., and Linke, R. A. 1984, *Ap. J. (Letters)*, **283**, L45.
 Thronson, H. A. 1983, *Ap. J.*, **264**, 599.
 Tielens, A. G. M. 1983, *Ap. J.*, **271**, 702.
 van den Bergh, S. 1984, *Ap. Space Sci.*, **102**, 295.
 Westbrook, W. E., Becklin, E. E., Merrill, K. M., Neugebauer, G., Schmidt, M., Willner, S. P., and Wynn-Williams, C. G. 1975, *Ap. J.*, **202**, 407.
 Wilson, W. J., Schwartz, P. M., and Epstein, E. E. 1973, *Ap. J.*, **183**, 871.
 Zuckerman, B. 1978, in *IAU Symposium 76, Planetary Nebulae: Observations and Theory*, ed. Y. Terzian (Dordrecht: Reidel).
 ———. 1981, *A.J.*, **86**, 84.
 Zuckerman, B., Palmer, P., Gilra, D. P., Turner, B. E., and Morris, M. 1978, *Ap. J. (Letters)*, **220**, L53.
 Zuckerman, B., Palmer, P., Morris, M., Turner, B. E., Gilra, D. P., Bowers, P. F., and Gilmore, W. S. 1977, *Ap. J. (Letters)*, **211**, L97.

G. R. KNAPP: Department of Astrophysical Sciences, Peyton Hall, Princeton University, Princeton, NJ 08544

MARK MORRIS: Department of Astronomy, Math Sciences Building, UCLA, Los Angeles, CA 90024